

Research on Deep-hole Drilling Quality of High-strength Steel With Slender Gun Drill

Jiabin Liang

Key Laboratory of Fundamental Science for Advanced Machining, Beijing Institute of Technology, Beijing100081, China

Li Jiao

Key Laboratory of Fundamental Science for Advanced Machining, Beijing Institute of Technology, Beijing100081, China

Pei Yan (✉ pyan@bit.edu.cn)

Beijing Institute of Technology

Minghui Cheng

Key Laboratory of Fundamental Science for Advanced Machining, Beijing Institute of Technology, Beijing100081, China

Tianyang Qiu

Key Laboratory of Fundamental Science for Advanced Machining, Beijing Institute of Technology, Beijing100081, China

Xibin Wang

Key Laboratory of Fundamental Science for Advanced Machining, Beijing Institute of Technology, Beijing100081, China

Research Article

Keywords: gun drill, deep hole, finite element simulation, drilling force, processing quality

Posted Date: March 22nd, 2021

DOI: <https://doi.org/10.21203/rs.3.rs-312959/v1>

License:  This work is licensed under a Creative Commons Attribution 4.0 International License.

[Read Full License](#)

Research on deep-hole drilling quality of high-strength steel with slender gun drill

Jiabin Liang^a, Li Jiao^a, Pei Yan^{a*}, Minghui Cheng^a, Tianyang Qiu^a, Xibin Wang^a

^a Key Laboratory of Fundamental Science for Advanced Machining, Beijing Institute of Technology, Beijing100081, China.

*Corresponding author: Tel: +86-10-6891-2716, Email: pyan@bit.edu.cn.

Abstract

There are a lot of problems exist in the processing of long and thin deep hole gun drilling of high strength steel, such as insufficient of the machining mechanism and characteristics of gun drilling, difficulty in selecting machining parameters, unknown influence mechanism of machining parameters on drilling force, drilling temperature and machining quality. In this paper, 42CrMo high strength steel is selected as the workpiece material. A numerical model of cutting force is established based on the mechanism of gun drill, and then the finite element simulation and processing test are carried out. The results show that the cutting force decreases with the increase of cutting speed, and increases with the increase of feed speed; the error between the theoretical and actual value is less than 10%. Cutting speed and feed speed have a great influence on machining quality, and the cutting fluid pressure mainly affects the surface roughness.

Keywords: gun drill; deep hole; finite element simulation; drilling force; processing quality.

1. Introduction

Deep hole drilling is an important machining method in the field of machining and manufacturing. With the development of machining technology and equipment manufacturing, deep hole drilling becomes more and more widely used and important ^[1]. At present, deep hole processing is mainly used in energy

and chemical industry, automobile engine, construction machinery and shipbuilding industry^[2]. However, it has become one of the most difficult machining technologies due to the complicated machining system and tool design, poor tool rigidity caused by large length-diameter ratio, and closed machining environment which is difficult to monitor.

Gun drill is the first processing system to realize large-scale and mature application in the field of deep hole processing. It is with the advantages of high processing efficiency, good processing quality and long tool life^[3]. As shown in Fig. 1, gun drill is composed with drill bit, drill pipe and drill handle. Generally, small diameter gun drills are formed by welding once, and the drill bit cannot be replaced. Larger diameter gun drills with blades can be replaced after the blades are worn out. The drill bit is the most important part of the gun drill, which undertakes the main drilling work. It is generally made of hard alloy and tool steel, with higher requirements on strength and wear resistance^[4]. The tip part of the drill bit is the cutting edge, and the circumference part is distributed with the guide block with the function of guiding and polishing, which can improve the machining accuracy of the hole. Generally, there is no need for reaming. In addition, since the gun drill has a unilateral cutting edge, the guide strip also has the function of balancing the radial cutting force on the cutting edge, and a reasonable guide block layout can keep the drilling process more stable. The drill pipe is used for chip removal and cutting fluid flow. It is usually made of seamless steel pipe. The drill pipe usually has a "V" groove structure, and the multi-blade gun drill has two V-grooves, through which the chip is discharged under the action of high pressure cutting fluid. The diameter of the drill pipe is slightly smaller than that of the bit, and the drill pipe is hollow inside, which is used for transmitting cutting fluid. The size design of the V-shaped groove and the through-oil hole should consider the rigidity of the drill pipe and the efficiency of through-oil and chip removal. The

drill handle is mainly used to transfer power and connect the fuel injection device. The model and geometry are adapted according to the machine tool selected.

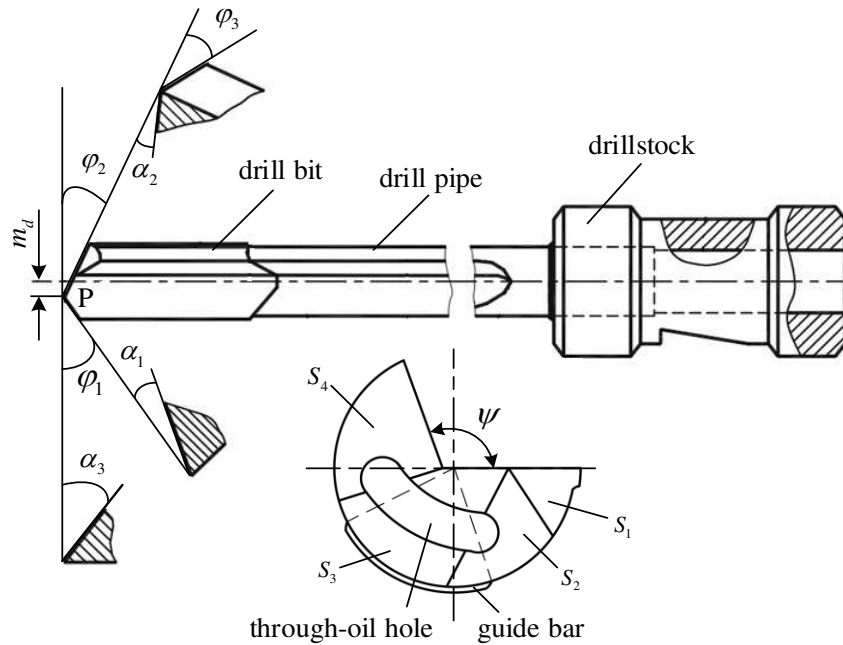


Fig. 1 Schematic diagram of gun drill

At present, some studies have been conducted in-depth on the improvement of processing structure, processing technology and drilling stability of gun drill. Viktor P et al.^[5] comprehensively analyzed the tool parameters of gun drill and the influence of machining parameters on tool life through a large number of experimental studies. Woon. K. S. et al.^[6] studied the influence of radius of the inner and outer edges of fillet on the straightness of the hole in the process of drilling thin-wall deep hole with gun drilling. Dirk Biermann et al.^[7] studied the influence of drill edge radius on drilling force, tool wear, tool life, chip length and surface roughness. Jung J^[8], Wang Y^[9] established a mathematical drilling force model of gun drills based on the energy principle and micro cutting tools, and the correctness of the model were verified by drilling experiments. Astakhov et al.^[10] studied the formation principle of trumpet mouth under gun drilling. Galitsky et al.^[11] established a tool life model for gun drilling by group data analysis method

(GMDH) including tool angle parameters and process parameters, which was a relatively perfect tool life prediction model. Klocke et al. ^[12] established a finite element analysis model of gun drilling process based on Deform-3D, and the simulation results were basically consistent with the experimental results by adjusting the radius of cutter blade circle and friction coefficient in the model. Yongguo Wang et al. ^[13] studied the corresponding relationship between the chip morphology and surface morphology under different tool wear conditions during gun drilling. On machining stability and straightness control, Alexander ^[14] studied the nonlinear bending vibration and torsional vibration in the gun drilling process, simplified the drill pipe into a continuous beam model, then proposed a new bending-torsional coupled vibration drilling model combined with the intermittent cutting theory. Tarng ^[15] developed a flutter identification system based on the ART2 neural network method, which could effectively identify the drill pipe vibration in the process of gun drilling. Kirsanov ^[2], Chin et al ^[16]. used finite element method to simulate the vibration and bending of drill pipe in the process of gun drilling.

However, there are still some problems in the gun drilling process, such as insufficient processing mechanism, lack of quantitative research on the influence of machining parameters, clamping error, tool parameters and other factors on machining quality, and low simulation accuracy. In this paper, the drilling force, drilling heat and machining quality of gun drilling are studied, especially for the influence of machining parameters on drilling force, drilling temperature and machining quality by combining theory, experiment and simulation.

2. Experimental procedures

A high strength steel 42CrMo round bar is used as the workpiece. The processing equipment adopted is the deep-hole gun drilling machine tool, Beijing Jinuo deep-hole equipment company. The tool is

German Cobalt Collar gun drill, the bit parameters are generally standard parameters, shown in Table 1.

Table 1 Bit parameters

External angle	Internal angle	Tool tip back angle	Groove angle	Inclination angle of diversion surface	Center distance of tool tip
40°	30°	38°	120°	20°	1 mm

The dynamometer used in this experiment is Type 9257 plate dynamometer produced by Kistler, Swiss. The main components include flat-panel dynamometer, signal collector, charge amplifier and the supporting PC DynoWare cutting force measurement and analysis software.

The drilling machine is a horizontal machine tool. The cutting fluid is pumped into the spindle and the drilling hole of the gun from the tail of the machine tool by the high pressure pump. It flows out through the head of the bit and discharges the chips into the chip container. The workpiece is fixed onto the dynamometer, and the dynamometer sensor collects the cutting force signals in the drilling process. After signal processing and amplification, the measured cutting force values are presented on DynoWare . The schematic diagram of test platform construction is shown in Fig. 2, and the experimental parameters are shown in

Table 2.

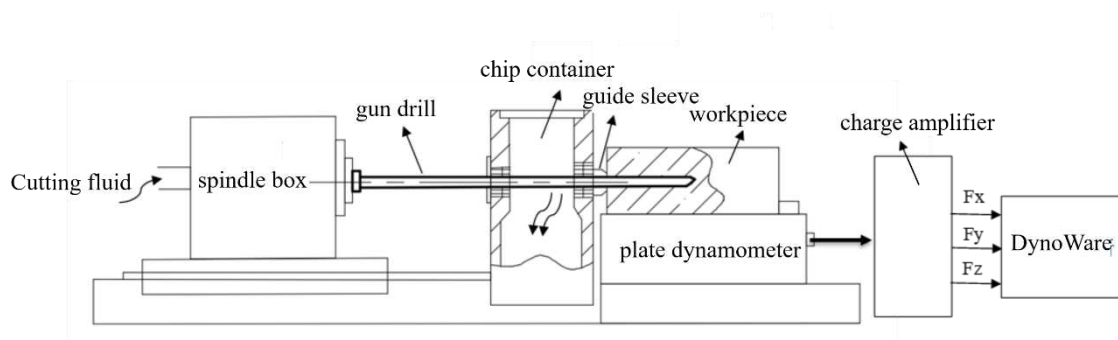


Fig. 2 Schematic diagram of gun drill drilling force measurement test platform

Table 2 Experimental parameters.

Cutting speed (rpm)	30 40 45 50 55 60
Feed speed ($\mu\text{m/r}$)	4 6 8 10 12
Cutting fluid pressure (MPa)	3 4 5 6
Hole depth (mm)	100
Hole diameter (mm)	4

After processing, the axis deviation, roundness and aperture size are measured using Hexagon Global Advantage coordinate measuring machine. The workpiece coordinate system is established based on the process datum (front and left side of the workpiece) corrected during machining. The diameter, roundness and center coordinates of the hole entrance-side and exit-side are measured respectively under the workpiece coordinate system, shown in Fig. 3.

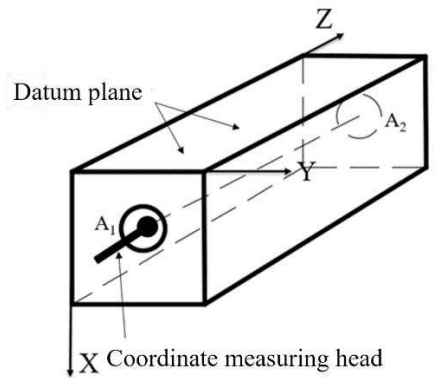


Fig. 3 Sketch of workpiece coordinate system

The surface morphology of the inner hole and the surface roughness were measured using Keyence 3D laser scanning microscope. In this paper, the machining hole is planed along the axis by wire cutting method, and then the surface topography is taken at three positions, i.e. 4 mm from the hole entrance, 4 mm from the middle of the hole and 4 mm from the exit of the hole, respectively. As shown in Fig. 4, each position was measured three times, and roughness was calculated in VK analysis software.



Fig. 4 Sketch map of surface roughness measurement position

3. Gun drilling thermodynamic coupling model

3.1 Mechanical numerical model

The force of the drill bit is complicated^[17], which can be divided into normal force, circumferential and axial friction force on the support surface of the guide strip, normal force and tangential friction force on the inner and outer cutting edges, and normal force formed by the cutting fluid on the outer diameter clearance surface. The overall stress analysis is shown in Fig. 5.

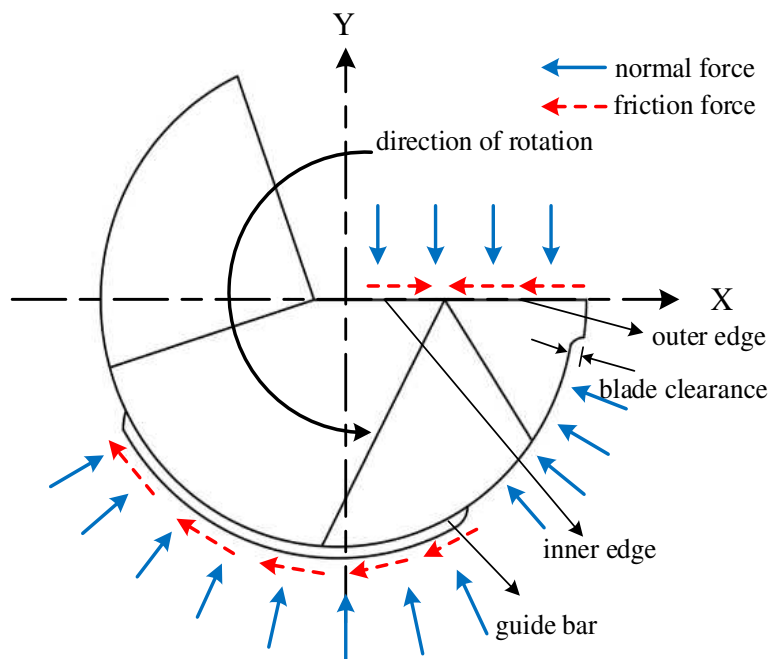


Fig. 5 Analysis of the overall stress of the drill bit

As shown in Fig. 6, the normal force on the support surface of the guide bar is simplified as R_p and the circumferential friction force is decomposed into R_{fx} and R_{fy} along X and Y directions. R_p can be described by the following formula :

$$R_p = p\delta r(\theta_2 - \theta_1) \quad (1)$$

Where, p is the unit normal force, r is the drilling radius, θ_1 and θ_2 is the starting angle and the ending angle of the drilling guide bar, δ is the contact area between the guide bar and the inner wall of the hole in the Z -axis direction. The R_p direction is at the center of the drill and the action point is $(\theta_1 + \theta_2)/2$.

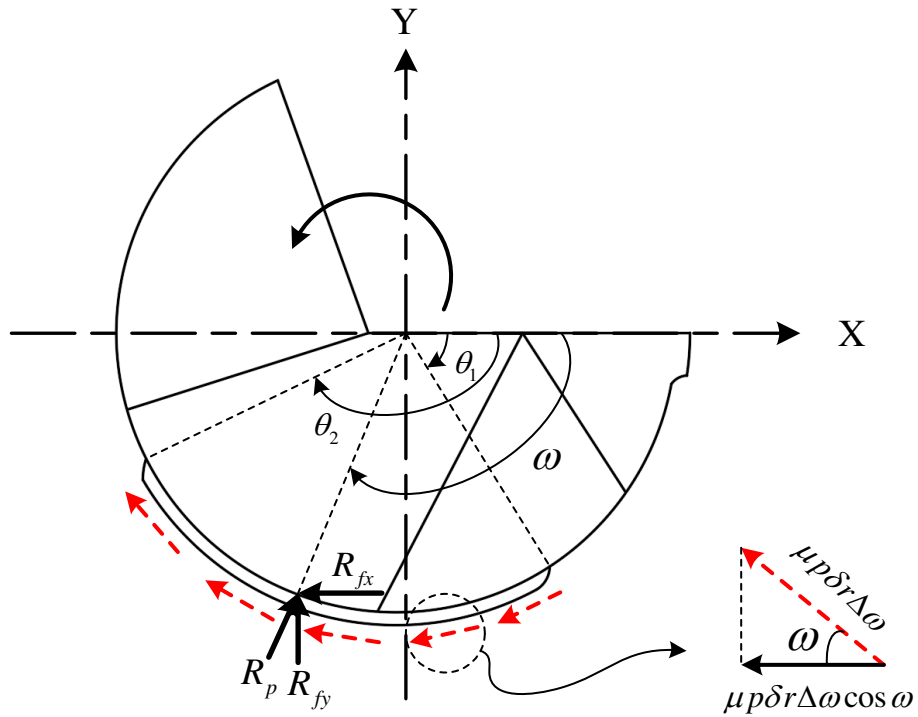


Fig. 6 Simplified force decomposition on guide bar

The circumferential friction force on the guide bar is decomposed into R_{fx} and R_{fy} , According to the triangle decomposition in the figure, when $\theta_1 \leq \omega \leq \pi/2$, the element's circumferential friction force dR_{fx} along the minus X axis, R_{fx} can be expressed as:

$$R_{fx} = \int_{\theta_1}^{\frac{\pi}{2}} \mu p \delta r \cos\left(\frac{\pi}{2} - \omega\right) d\omega = \int_{\theta_1}^{\frac{\pi}{2}} \mu p \delta r \sin(\omega) d\omega = \mu p \delta r \cos \theta_1 \quad (2)$$

When $\pi/2 \leq \omega \leq \theta_2$, dR_{fx} along the minus X axis, R_{fx} can be expressed as:

$$R_{fx} = \int_{\frac{\pi}{2}}^{\theta_2} \mu p \delta r \cos\left(\omega - \frac{\pi}{2}\right) d\omega = \int_{\frac{\pi}{2}}^{\theta_2} \mu p \delta r \sin(\omega) d\omega = -\mu p \delta r \cos \theta_2 \quad (3)$$

Where, μ is the friction coefficient, ω is the angle variable.

Therefore, at the top $\theta_1 \leq \omega \leq \theta_2$, R_{fx} can be expressed as:

$$R_{fx} = \mu p \delta r (\cos \theta_1 - \cos \theta_2) \quad (4)$$

Similarly, R_{fy} along the Y axis, and the expression of R_{fy} is:

$$R_{fy} = \mu p \delta r (1 - \sin \theta_2) - \mu p \delta r (1 - \sin \theta_1) = \mu p \delta r (\sin \theta_1 - \sin \theta_2) \quad (5)$$

Suppose the axial friction coefficient on the guide bar is μ_L , the axial friction force R_t on the guide bar can be expressed as:

$$R_t = \int_{\theta_1}^{\theta_2} \mu_L p \delta r d\omega = \mu_L p \delta r (\theta_2 - \theta_1) = \mu_L R_p \quad (6)$$

Due to the special single-edge structure of the gun drill, the cutting speed at each point of the inside and outside edges is different, and the cutting force distributed along the cutting edge is un-uniform. Therefore, the internal and external cutting edges are divided into countless micro elements by the micro element method, and each micro element can be regarded as a cutting element. If the number of micro-element is large enough and the area of micro-element is small enough, the cutting speed on each micro-element can be considered as unchanged^[18]. After the cutting force on each micro-element is obtained, the cutting force on the whole cutting edge can be obtained by integrating along the cutting edge.

Then the normal force F_{n1} and friction force F_{f1} on the outer edge can be expressed as:

$$F_{n1} = \sum_{j=1}^m K_n(j) dA_1(j) = \sum_{j=1}^m t_{c1} K_n(j) dx(j) \quad (7)$$

$$F_{f1} = \sum_{j=1}^m K_f(j) dA_1(j) = \sum_{j=1}^m t_{c1} K_f(j) dx(j) \quad (8)$$

Similarly, the normal force F_{n2} and friction force F_{f2} on the inner edge can be expressed as:

$$F_{n2} = \sum_{j=1}^n K_n(j) dA_2(j) = \sum_{j=1}^n t_{c2} K_n(j) dx(j) \quad (9)$$

$$F_{f2} = \sum_{j=1}^n K_f(j) dA_2(j) = \sum_{j=1}^n t_{c2} K_f(j) dx(j) \quad (10)$$

In the process of gun drilling, the cutting force mainly comes from the decomposition of the normal force and friction force on the guide bar and cutting edge as well as the clearance water pressure in XYZ directions. According to the principle of force balance, the forces are decomposed in X and Y directions, seen as follows ^[9]:

$$F_{n1} + F_{n2} = R_{fy} + R_p \sin\left(\frac{\theta_1 + \theta_2}{2}\right) + R_h \sin\left(\frac{\theta_0 + \theta_1}{2}\right) \quad (11)$$

$$R_p \cos\left(\pi - \frac{\theta_1 + \theta_2}{2}\right) = R_{fx} + F_{s1} - F_{s2} + R_h \cos\left(\frac{\theta_0 + \theta_1}{2}\right) \quad (12)$$

For convenience of calculation, let $\xi = \frac{\pi n}{30}$, $\xi_{a1} = a_2 + a_4 + \ln t_{c1} + 1$, $\xi_{b1} = b_2 + b_4 + \ln t_{c1} + 1$, $\xi_{a2} = a_2 + a_4 + \ln t_{c2} + 1$ and $\xi_{b2} = b_2 + b_4 + \ln t_{c2} + 1$. Where, t_c are actual cutting thickness; , φ_1 and φ_2 are the outer and inner angles of the gun drill respectively; $a_0 - a_4$ and $b_0 - b_4$ are model calibration coefficients. In combination with vertical (11) and (12), the expression of positive pressure R_p on the support surface of the guide bar is obtained as follows:

$$R_p = \frac{-\tan\left(\frac{\theta_1 + \theta_2}{2}\right) (F_{s1} - F_{s2}) - (F_{n1} + F_{n2}) - r \cos\left(\frac{\theta_1 + \theta_2}{2}\right)}{\tan\left(\frac{\theta_1 + \theta_2}{2}\right) [F_{fx} (\cos \theta_1 - \cos \theta_1) + F_{fy} (\sin \theta_1 - \sin \theta_1)]} \quad (13)$$

During drilling, the main cutting force is feed resistance. Feed force F_Z is mainly composed of two

parts: the friction force R_t along the Z direction of the guide bar and the component force F_t of the friction force on the cutting edge in the Z direction. Here $F_t = F_{t1} + F_{t2} = F_{f1} \cos \varphi_1 + F_{f2} \cos \varphi_2$, so F_z can be represented as:

$$\begin{aligned}
F_z &= R_t + F_t = \mu_L R_p + F_{f1} \cos \varphi_1 + F_{f2} \cos \varphi_2 \\
&= e^{b_0} t_{c1}^{b1} (1 - \sin \gamma_n)^{b3} (f/\xi)(1/\xi_{b1}) (m_d \xi)^{\xi_{b1}} \cos \varphi_2 + \\
&\quad e^{b_0} t_{c2}^{b1} (1 - \sin \gamma_n)^{b3} (f/\xi)(1/\xi_{b2}) \left[(r\xi)^{\xi_{b2}} - (m_d \xi)^{\xi_{b2}} \right] \cos \varphi_1 + \mu_L R_p
\end{aligned} \tag{14}$$

3.2 Thermodynamic coupling finite element model

Due to the small heat dissipation space in the drilling process, the workpiece and tool absorb most of the cutting heat, and the chip takes away only about 30% of the heat. The workpiece expansion caused by the cutting heat will affect the machining precision, especially in the deep hole machining, the cutting heat has a great influence on the diameter deviation of the machining hole ^[19].

In this paper, the finite element model of gun drilling is established by Deform-3D. In this model, the radius of the cutting edge circle is not considered, and it is assumed to be absolutely sharp. The effect of the cutting fluid and the through-oil hole are also without considered. In order to facilitate the grid division, the through-oil hole is removed and simplified. For reduce the number of grids and improve the computational efficiency, only a small part of bits involved in cutting are retained in the simulation. The shapes of the meshed workpiece and cutter are shown in Fig. 7. The material model of the workpiece is defined as the Johnson-Cook model, and the parameters are shown in Table 3^[14].

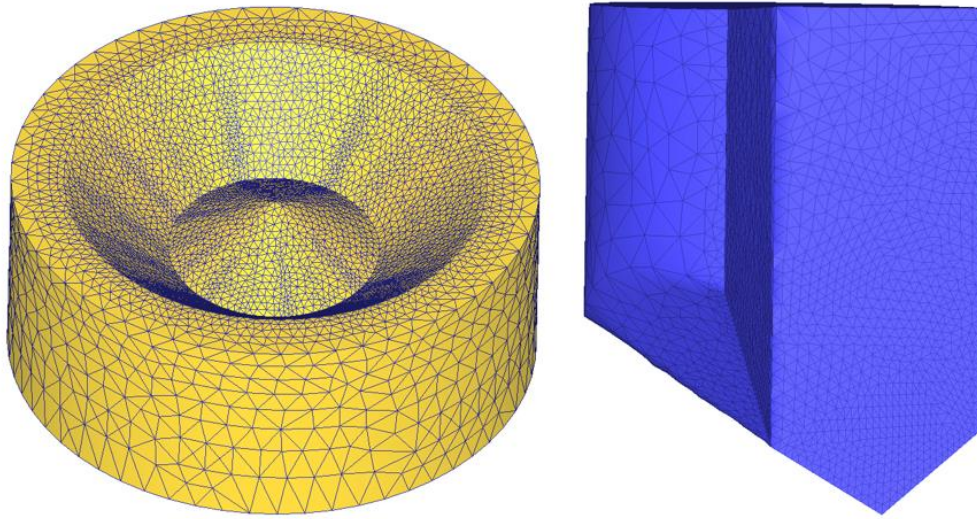


Fig. 7 Effect drawing of mesh division of workpiece and tool

Table 3 J-C constitutive model parameters of 42CrMo

A (MPa)	B (MPa)	C	n	m	T_m (°C)	T_r (°C)
595	580	0.023	0.133	1.03	1820	20

For the contact conditions between the workpiece and the tool, the contact tolerance is set as 0.0002, and the contact calculation method is penalty function method. The friction type is shear friction, and the average friction coefficient in the calculation is set as 0.4. The heat transfer coefficient between the workpiece and the tool is determined by the pressure, sliding speed, contact temperature, etc. As shown in Table 4 ^[20], in order to facilitate the simulation, the heat transfer coefficient between the workpiece and the tool is determined as a function of pressure. The tool wear model is Usui model, which is applicable to simulate the tool wear in cutting, with the empirical coefficient $a = 1 \times 10^{-7}$, $b = 855$.

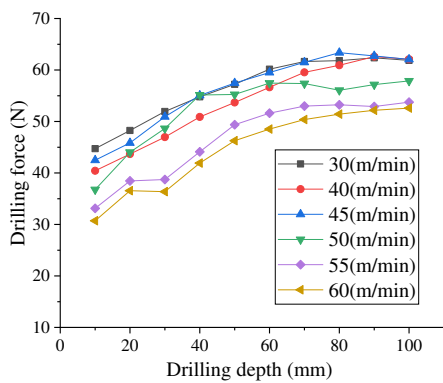
Table 4 Heat transfer coefficient between workpiece and tool

Contact pressure (MPa)	0	30	180	300	420	600
Heat transfer coefficient (N/mm \cdot s \cdot °C)	5	18	87	222	410	500

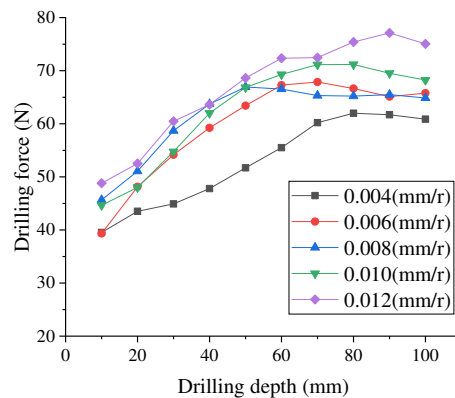
4. Experiment results and discussion

4.1 Thermodynamic coupling model results of drilling

Fig. 8 shows the variation curve of drilling force with hole depth at each cutting speed and feed speed. Because the radial cutting forces F_x and F_y fluctuate up and down on the coordinate axis, and the average value is close to 0. This paper mainly analyzes the feed resistance F_z , and the drilling forces mentioned below all represent F_z . At the same time, the speed of the maximum diameter on the outer edge of the gun drill is selected as the cutting speed. With the increase of drilling depth, the drilling force gradually increases. When the hole is relatively shallow, the increasing speed and amplitude of the drilling force are relatively large, which may be related to the friction force. With the increase of hole depth, the drilling force increases by more than 30%, indicating that the drilling state is not always stable in the process of deep hole drilling. This leads to the difference of drilling force in different depths of holes, and it will also affect the dimensional accuracy and surface quality at different depths. The variation of cutting force can be used as an effective factor to represent the variation of cutting state.



(a)



(b)

Fig. 8 Comparison of drilling force with hole depth under different cutting speed (a) and feed speed (b)

The values of each cutting speed and feed speed were substituted into Equation (24) to calculate the predicted values of the theoretical model of drilling force. Meanwhile, the average of the measured values was taken and the comparison curve of the predicted and measured values was drawn according to the result data, as shown in Fig. 9. It can be seen that with the increase of cutting speed, the predicted value of cutting force decreases gradually. In addition to the results under 45 m/min, the measured values also show a general trend of decreasing with the increase of cutting speed, and the decreasing speed is faster under high speed. This indicates that increasing spindle speed can reduce the drilling feed resistance and improve the stability of machining system. At the same time, according to the theoretical results, the relationship between drilling force and feed velocity is close to linear growth. Although there is no obvious linear relationship between experimental values, the overall size of drilling force increases with the increase of feed speed. The main reason is that the increase of feed speed f leads to the increase of cutting thickness t_c and instantaneous cutting area, which leads to the increase of tool load and axial feed resistance. The variation trend is basically the same, with the maximum error about 10%, which verifies the correctness of the established mathematical model of drilling force.

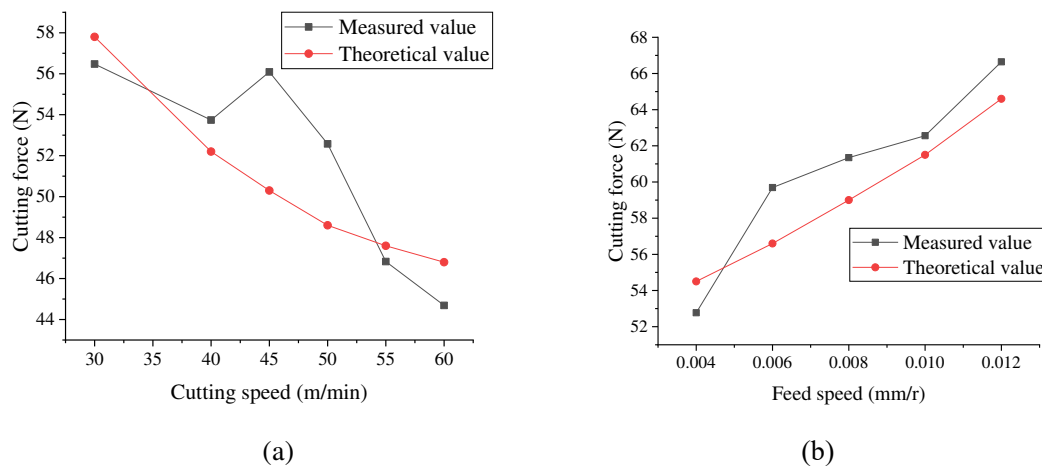


Fig. 9 Comparison of drilling force and cutting speed (a) and feed speed (b)

Fig. 10 shows the surface temperature field distribution of workpiece and cutting tool at time step=900. The highest temperature of the workpiece at the same time is higher than that of the tool. The main reasons are as follows: first, the temperature rise is different due to the different thermal characteristics of the two materials; second, it takes a certain time for the temperature to be transferred from the workpiece to the tool, and there is a heat loss in the transfer process. The highest temperature of the workpiece is concentrated in the cutting part, where the chip and the workpiece just separated, and the temperature decreases gradually along the processed surface and the chip surface. The temperature on the chip is higher than that on the machined surface, and the temperature field distribution on the workpiece is basically consistent with the theoretical analysis. The highest temperature of the tool appears on the tip and the inner and outer edges, and the temperature field is distributed symmetrically on the flank and rake face with the inner and outer cutting edges as the center, with a large temperature gradient. The thermal load on the outer edge is significantly higher than that on the inner edge, which is related to the larger average cutting speed of the outer edge. The cutting temperature of the outer edge is higher than that of other positions due to the largest contact area between the cutting surface and the chip. As the cutting depth increases, friction occurs between the outer cylinder of the drill bit and the inner surface of the hole, and the temperature also begins to appear on the outer cylinder.

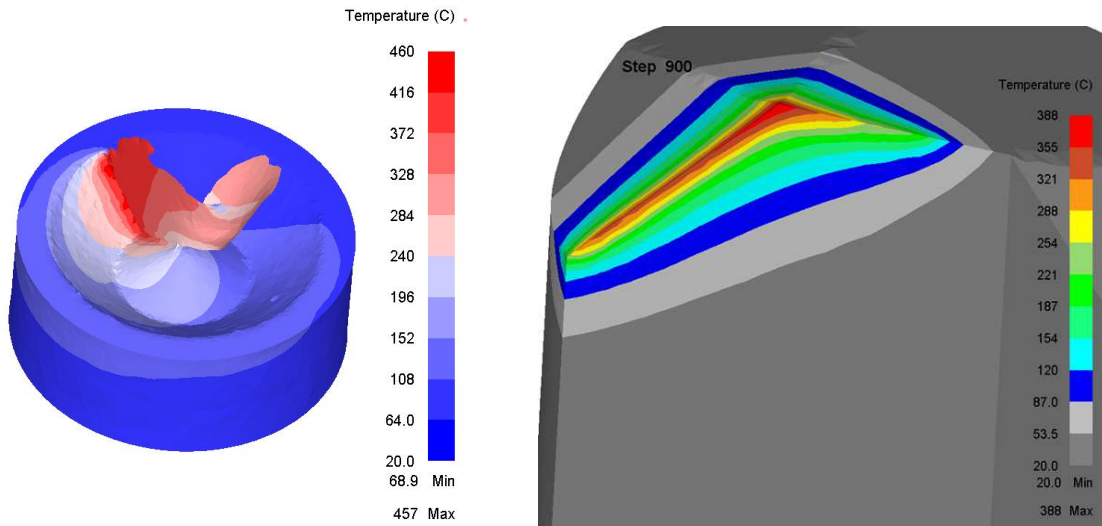


Fig. 10 Temperature distribution nephogram of workpiece and tool at step = 900

As shown in Fig. 11, the workpiece cutting area is divided along depth to analyze the distribution of temperature field. It can be seen that the temperature starts from the cutting area and gradually decreases along the depth, indicating that the drilling heat is transferred from the cutting area to the workpiece interior, which cause the workpiece interior temperature to rise. By magnifying the chip root position, it can be seen that the temperature contour distribution is dense and the temperature gradient is large. At the same time, the distribution of temperature field also exists in the area between the chip and the rough surface (the first deformation area), indicating that the cutting heat is generated in this area, which is consistent with the mechanism of cutting heat generation.

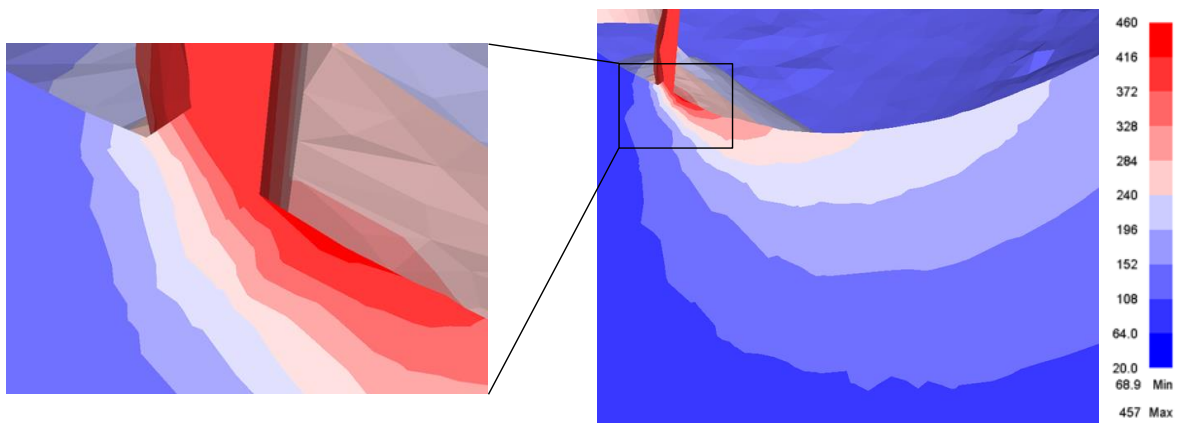


Fig. 11 Distribution of workpiece temperature field along depth

The vertical cutting edge dissects the bit along the axis are shown in Fig. 12, .Compared with the workpiece, the temperature distribution on the bit is more concentrated, and the heat transfer range along the axis is shallow. It shows that in the process of drilling, a lot of heat is gathered near the drill tip and cutting edge, and the heat diffuses slowly to the inside of the drill bit. The heat dissipation mainly depends on the heat dissipation medium. It can be seen that good cutting fluid cooling is important for gun drilling. It can be predicted from the characteristics of the cutting temperature field that the wear of the gun drill should mainly occur on the front surface near the outer edge and tip.

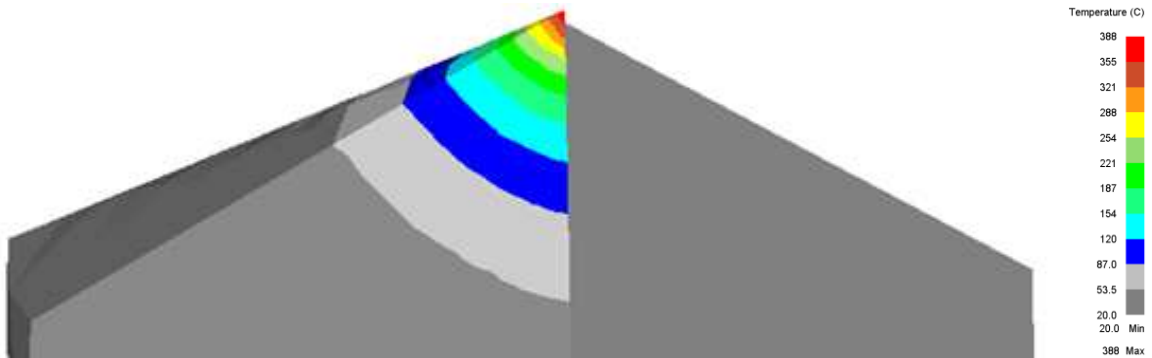


Fig. 12 Cloud chart of temperature field along axial depth on bit

Three reference points P1, P2 and P3 were selected in the internal non-cutting area of the workpiece, and the temperature at the three points was tracked with time to obtain the curve, shown in Fig. 13. The closer the point to the cutting area, the higher the temperature is, and vice versa. According to the tool position corresponding to each section of the curve, the tool rotation and feed constantly change the relative position of the cutting area and the reference point, which leads to the step-wise increase of the temperature curve at the reference points. The step effect of the temperature curve at point P1 closest to the cutting area is the most obvious, while the time of the inflection point of temperature mutation is later at point P3 with a small amplitude due to the buffering and delay of heat transfer.

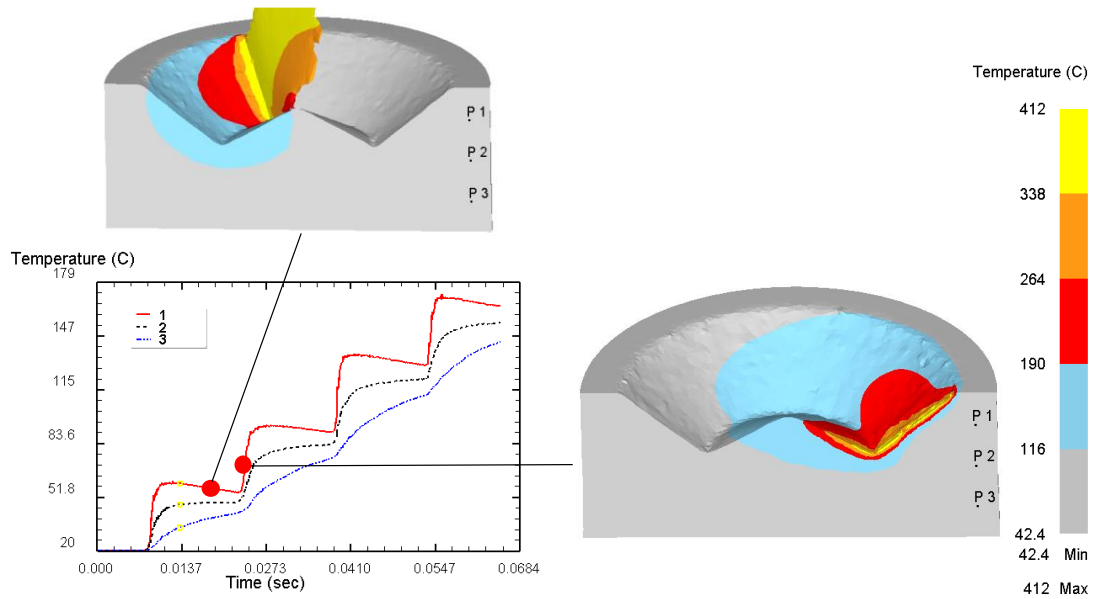


Fig. 13 Temperature variation curve of internal reference point of workpiece

Similarly, a reference point P1 near the tip on the rake face is selected to track the temperature as time changes, and the curve is shown in Fig. 14. It can be seen that when the tool just cuts into the workpiece, the temperature at this point increases sharply and rises slowly in a diagonal line after about 0.014s. The change of temperature reflects the process of cutting from the initial state to the stable state.

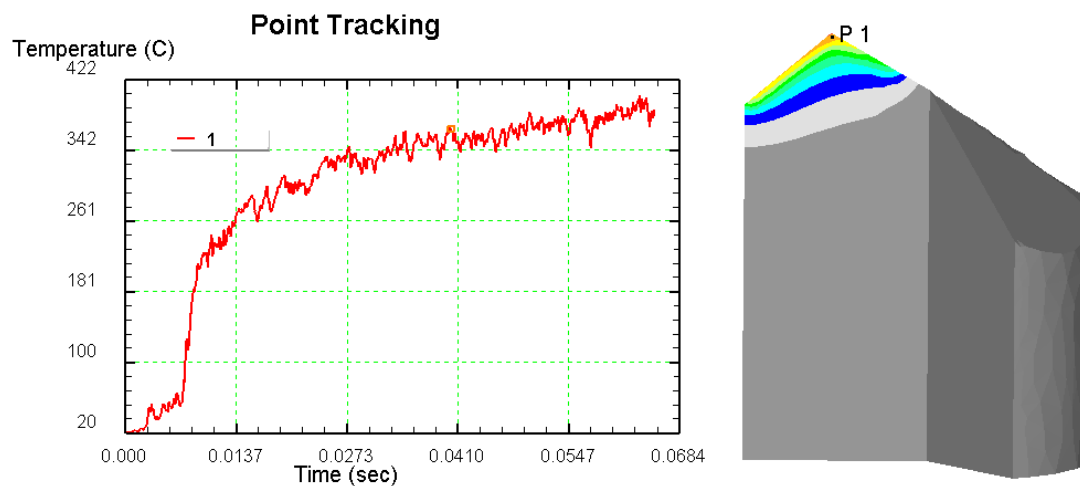


Fig. 14 Cutting temperature curve with time at drill point

In this paper, the temperature at the drill tip was used to represent the cutting temperature to extract the temperature simulation results under each parameter, and the average temperature between (0.02-0.05)

s was calculated to draw the graph shown in Fig. 15. As the cutting speed increases, the cutting temperature shows a linear trend of increasing, and the growth rate is faster at high feed speed. When the cutting speed is constant, the cutting temperature increases with the increase of feed speed, and it is sensitive to the change of the feed speed at low feed rate.

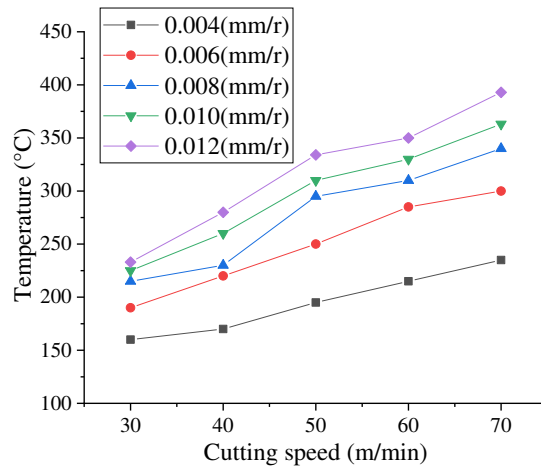


Fig. 15 Comparison of cutting temperature and cutting speed under different feed speed

4.2 Effect of processing parameters on processing quality

In the process of gun drilling, there are problems of drill pipe length, poor rigidity, gap between drill bit and guide sleeve, drill pipe vibration, rotary vibration in the guide sleeve clearance repeatedly, which lead to the deviation between drill hole diameter and tool diameter and hole roundness error. Tool wear, cutting heat and other factors also lead to hole inlet and outlet diameter deviation.

It can be seen from Fig. 16 and Fig. 17 that the diameter of entrance of the hole should be larger than that of the exit. With the increases of cutting speed, the diameter of the exit decreases more and more, and that of the entrance also fluctuates to a certain extent, but the range is relatively small. The diameter deviation of the entrance and exit shows a linear rising trend with the increases of cutting speed. The diameter change at the entrance can be attributed to the wear of the guide bar and the random error of

measurement. The diameter of the hole outlet is obviously smaller than the gun drill, which is related to the cutting temperature. According to the simulation analysis, in the process of gun drilling, the drilling temperature is relatively high, and increases with the increase of cutting speed. A large amount of cutting heat is transferred to the workpiece, and the temperature near the hole is high, and rises rapidly due to the slow heat dissipation of the workpiece with larger hole depth. Due to the effect of thermal expansion and cold contraction, the workpiece expanded during drilling, and then its temperature gradually returned to room temperature after drilling, leading to the shrinkage of the material and the reduction of the hole diameter. The faster the cutting speed, the higher the cutting temperature. The obvious effect of heat expansion and cold contraction results in the hole inlet and outlet diameter deviation.

It can be seen from the roundness error curve in Fig. 18 that the roundness error at the entrance of the hole is smaller than the exit, which is related to the inconsistency of the internal shrinkage rate of the material. With the increase of feed velocity, the diameters of inlet and outlet are with some fluctuation, but the variation range is small, and the diameter deviation has little change. The roundness error of the inlet is smaller than that of the outlet, but the feed velocity has little influence on the diameter error and roundness error of the inlet and outlet. With the increase of cutting fluid pressure, the hole exits basic remain stable, the diameter difference of the inlet and outlet is less. That is because as the cutting fluid pressure and flow rate increases, the cooling performance of gun drill system reduces the cutting temperature. But the pressure strengthen the pipe eddy effect and the drill string vibration, resulting in the hole roundness error increases.

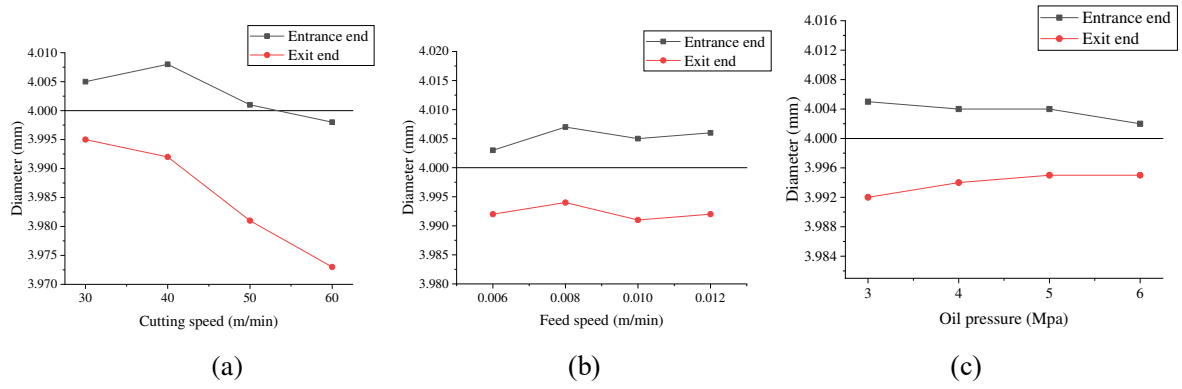


Fig. 16 Comparison of diameter of hole inlet and outlet and cutting speed (a), feed speed (b) and oil pressure (c)

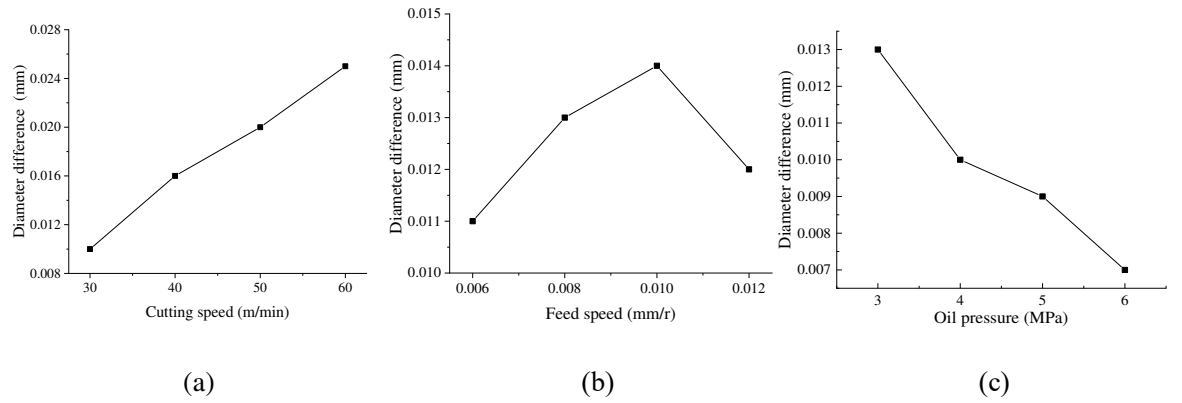


Fig. 17 Comparison of diameter difference between inlet and outlet and cutting speed (a), feed speed (b) and oil pressure (c)

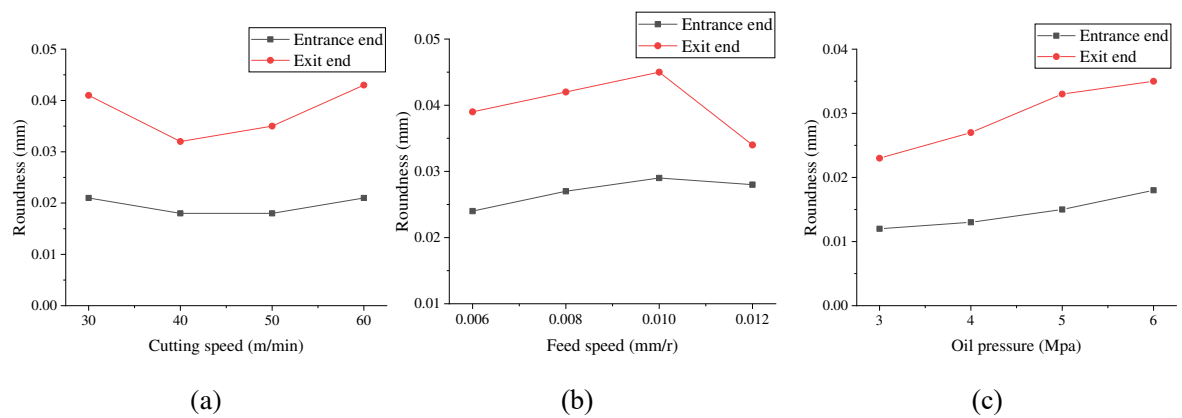


Fig. 18 Comparison of roundness of hole inlet and outlet and cutting speed (a), feed speed (b) and oil pressure (c)

The axis deviation of long and thin deep holes is the most important parameter to represent their machining quality. For spatial cross holes with high position accuracy, the axis deviation will lead to the exit position deviation, which will affect the intersection of the hole system and oil transfer efficiency, and even lead to the scrap of the workpiece. Axis deviation is mainly caused by the bending of the drill, which is related to machining parameters, clamping accuracy, vibration and other factors.

Fig. 19 shows the axis deviation of deep hole under various drilling parameters. It can be seen that the deviation in X direction (vertical direction) is much greater than that in Y direction (horizontal direction), and the linear deviation of hole mainly depends on the variation of X-direction, which indicated that the bending of gun drill mainly occurs in the gravity direction, and the deviation of hole axis is around 0.06 mm. With the increase of cutting speed, the deviations of Y axis and X axis show a slow rising trend. This is caused by the increase of spindle speed, which decreases the machining stability of the drill pipe and aggravates the vibration. At the same time, the increase of speed leads to the increase of feed per minute, which increases the resistance of drilling feed and finally makes the drill pipe more prone to bending. With the increase of feed speed, the Y-direction deviation shows a slow growth trend, and the X-direction deviation fluctuates up and down, with a slight increase in the overall value. The change of linear deviation is basically consistent with the X-direction deviation. This indicates that due to the increase of feed speed, the axial feed resistance of drilling increases, which leads to the increase of the bending degree of drilling gun, but the overall effect is small. With the increase of cutting fluid pressure, the Y-direction deviation of hole axis increases, and the X-direction deviation also increases slightly. The variation of cutting fluid pressure mainly affects the axis Y deviation, and this is related to the increase of pressure and vortex effect of cutting fluid in the hole. Generally, the cutting fluid pressure has little influence on the

axis deviation of the hole.

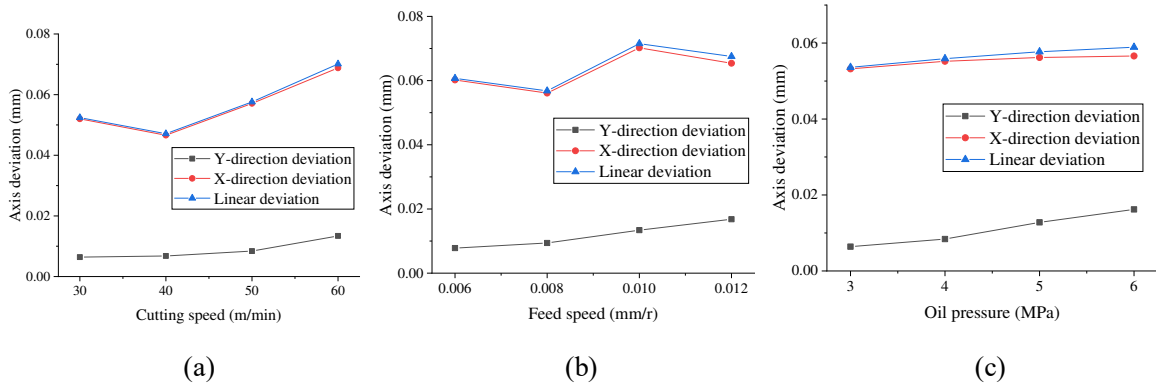


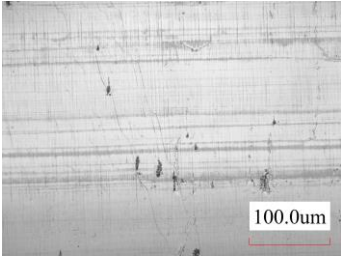
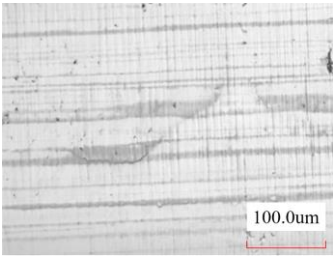
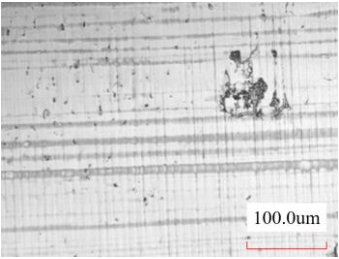
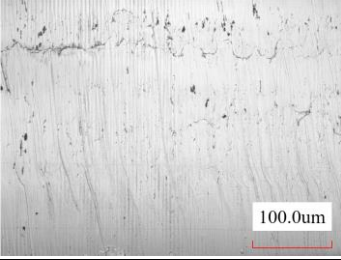
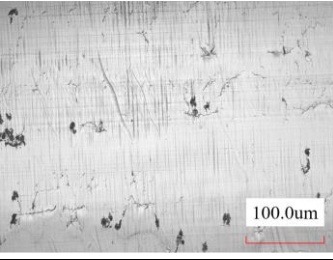
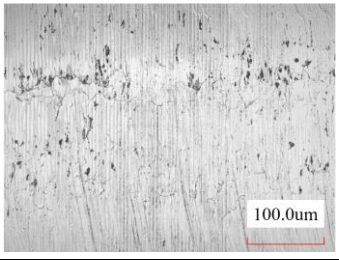
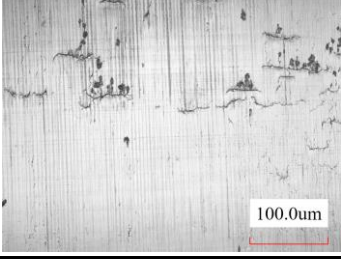
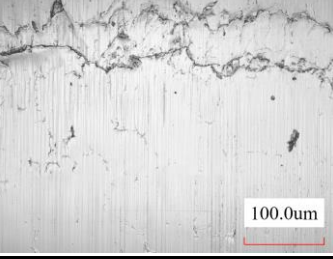
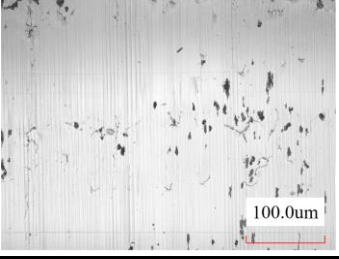
Fig. 19 Comparison of axis deviation and cutting speed (a), feed speed (b) and oil pressure (c)

The surface micro morphologies of each hole measured position are shown in Table 5. It can be seen from the micro morphology of the processed hole that the surface of the hole has surface defects such as cracks, scratches, dense grooves and pits formed by material hard points falling off. With the decrease of oil pressure, there are more scratches on the processed hole surface, and the surface will be rougher. In gun drilling, the influence of tool deflection angle and edge circle radius on the surface of machined hole is relatively small, while the friction and polishing of the guide strip on the machined hole wall and the scraping of the chip have a great influence.

It can be seen from Fig. 20 that with the increase of cutting speed, the surface roughness of machined hole gradually increases. The reason is that with the increase of cutting speed, cutting fluid is easy to form eddy at the bottom of the hole, resulting in the reduction of chip discharge performance. This increases the chip scraping on the machined surface, and small chips and hard point particles of the workpiece are easy to get stuck in the gap between the guide strip and the hole wall. The faster the speed, the greater damage to the hole wall. With the feed rate increases from 0.006 mm /r to 0.01 mm /r, the surface roughness of the machining hole increases slowly, then it increases rapidly over 0.01 mm /r. That is because the chip

thickness and length increases with feed speed, resulted in the difficulty of chip breaking increases. The friction of chip on the surface of the processed hole increases, leading to the increase of surface roughness. According to the test results, the influence of chip length and thickness on the surface roughness is enhanced after the feed rate is 0.01mm /r. Therefore, for the long and thin deep hole processing with high surface quality requirements, the feed rate should not exceed 0.01mm /r. With the increase of cutting fluid pressure, the chip length gradually becomes shorter, and the chip form also changes from a seriously deformed long tapered strip to a regular short spiral, indicating that the chip discharge ability of the processing system is enhanced. Chip discharge is smooth without blocking, and the friction of the chip on the surface is reduced, so the surface roughness is reduced.

Table 5 Micro surface morphology of each hole measured position

	Entrance end	Middle end	Exit end
1			
2			
3			

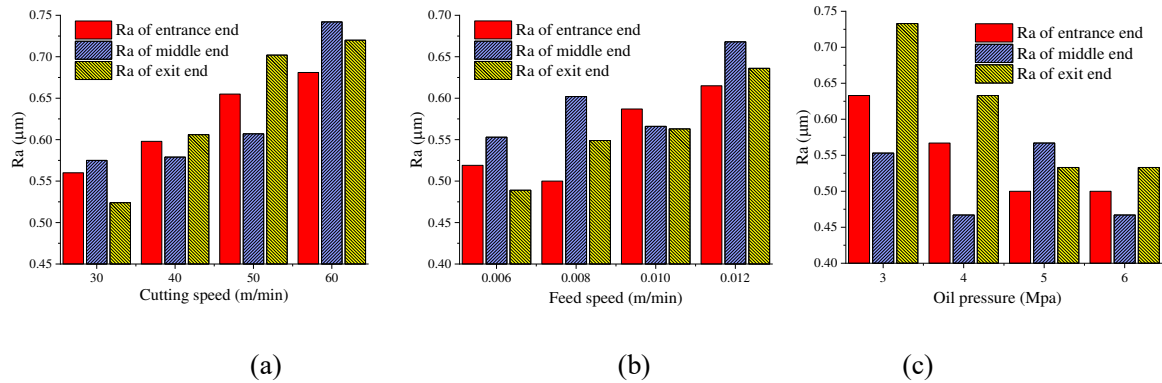
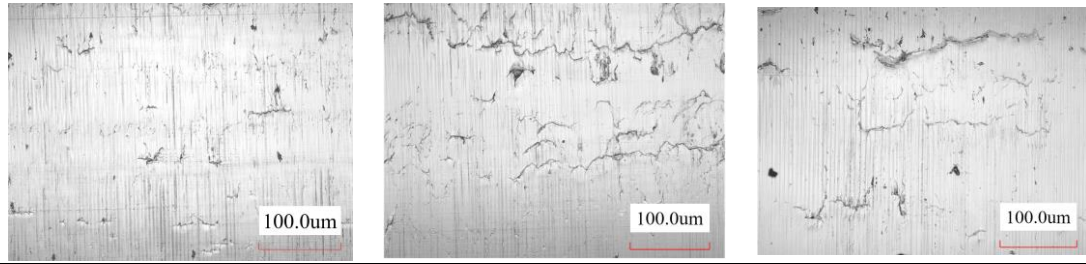


Fig. 20 Comparison of surface roughness and cutting speed (a), feed speed (b) and oil pressure (c)

5. Conclusion

In this paper, 42CrMo high-strength steel is selected as the experimental material. Based on the drilling mechanism of gun drilling, combined with finite element simulation and processing test, the influence of processing parameters on drilling force, drilling temperature and processing quality is analyzed. The main contents of the study are summarized as follows:

(1) Numerical model analysis and experimental verification of drilling force are carried out. The drilling force tends to increase rapidly and then become stable with the increase of hole depth, and decreases with the increase of cutting speed and increases with feed speed. The maximum error between experimental data and theoretical value is less than 10%.

(2) The finite element simulated temperature and temperature gradient near the chip root are the largest, and the temperature in the uncut area of the workpiece rises in a stepped manner with the tool feed.

The temperature and temperature gradient near the cutting edge and the drill tip are maximum, and increases with the increase of cutting speed and feed speed, with the cutting speed is the main influencing factor.

(3) Cutting speed and feed speed have a great influence on the machining quality, and cutting fluid pressure mainly affects surface roughness.

Funding

This work was supported by the National Key Research and Development Program of China, China [Grant number 2020YFB2010600] and National Natural Science Foundation of China, China [Grant number 52075040].

Data availability We confirm that data is open and transparent.

Competing interests The authors declare that they have no competing interests.

Ethical approval Not applicable.

Consent to participate Not applicable.

Consent to publish Not applicable.

References

- [1] Zhang X, Tnay GL, Liu K, Kumar AS. (2018) Effect of apex offset inconsistency on hole straightness deviation in deep hole gun drilling of Inconel 718. *International Journal of Machine Tools and Manufacture*,125:123-132. doi: 10.1016/j.ijmachtools.2017.11.011
- [2] Kirsanov SV, Tsygankov RS, Tukhfatullin BA. (2017) Automated Calculation of Shaft Flexure for a Gun Drill. *Russian Engineering Research*,7:581-584. doi:
- [3] Neo DWK, Liu K, Kumar AS. (2020) High throughput deep-hole drilling of Inconel 718 using PCBN gun drill. *Journal of Manufacturing Processes*,57:302-311. doi: 10.1016/j.jmapro.2020.06.043
- [4] Zhang X, Tnay GL, Liu K, Kumar AS. (2018) Effect of apex offset inconsistency on hole straightness deviation in deep hole gun drilling of Inconel 718. *International Journal of Machine Tools and Manufacture*,125:123-132. doi: 10.1016/j.ijmachtools.2017.11.011
- [5] Astakhov VP, Galitsky VV. (2008) The combined influence of various design and process parameters of gundrilling on tool life: experimental analysis and optimization. *The International Journal of Advanced Manufacturing Technology*,36:852-864. doi: 10.1007/s00170-006-0903-x
- [6] Woon KS, Chaudhari A, Rahman M, Wan S, Kumar AS. (2014) The effects of tool edge radius on drill

-
- deflection and hole misalignment in deep hole gun drilling of Inconel-718. *CIRP Annals*,63:125-128. doi: 10.1016/j.cirp.2014.03.075
- [7] Biermann D, Wolf M, Aßmuth R. (2012) Cutting Edge Preparation to Enhance the Performance of Single Lip Deep Hole Drills. *Procedia CIRP*,1:172-177. doi: 10.1016/j.procir.2012.04.030
- [8] Jung J, Ke F. (2007) A gun drilling force system. *International Journal of Machine Tools and Manufacture*,47:1276-1284. doi: 10.1016/j.ijmactools.2006.08.018
- [9] Wang Y, Jia W, Zhang J. (2014) The force system and performance of the welding carbide gun drill to cut AISI 1045 steel. *The International Journal of Advanced Manufacturing Technology*,74:1431-1443. doi: 10.1007/s00170-014-6072-4
- [10] Astakhov VP. (2002) The mechanisms of bell mouth formation in gun drilling when the drill rotates and the workpiece is stationary. Part 2: the second stage of drill entrance. *International journal of machine tools & manufacture*,42:1145-1152. doi: 10.1016/S0890-6955(02)00051-2
- [11] Astakhov VP, Galitsky VV. (2005) Tool life testing in gun drilling: an application of the group method of data handling (GMDH). *International Journal of Machine Tools and Manufacture*,45:509-517. doi: 10.1016/j.ijmactools.2004.09.003
- [12] Klocke F, Abouridouane M, Gerschwiler K, Lung D. (2011) 3D Modelling and Simulation of Gun Drilling. *Advanced Materials Research*,223:12-19. doi: 10.4028/www.scientific.net/AMR.223.12
- [13] Wang Y, Yan X, Li B, Tu G. (2012) The study on the chip formation and wear behavior for drilling forged steel S48CS1V with TiAlN-coated gun drill. *International Journal of Refractory Metals and Hard Materials*,30:200-207. doi: 10.1016/j.ijrmhm.2011.08.010
- [14] Gousskov AM, Butcher EA, Voronov SA, Sinha SC. (2005) NONLINEAR FLEXURAL-TORSIONAL VIBRATIONS OF A GUNDRILLING TOOL. *ASME 2005 International Design Engineering Technical Conference*. doi:
- [15] Tarng YS, Li TC. (1995) Adaptive Pattern Recognition of Drilling Chatter. *Journal of Materials Processing Technology*:247-253. doi:
- [16] Chin J, Sheu S. (2007) Strengths and weaknesses of finite element modeling deep hole drilling as compared with beam and column equations. *The International Journal of Advanced Manufacturing Technology*,32:229-237. doi: 10.1007/s00170-005-0332-2
- [17] Li L, He N, Hao X, Yang Y. (2019) Deep-hole gun drilling mechanics model of Ti6Al4V alloy based on Johnson and Cook flow stress model. *The International Journal of Advanced Manufacturing Technology*,104:4497-4508. doi: 10.1007/s00170-019-04244-6
- [18] AR W. (1985) Drilling model for cutting lip and chisel edge and comparison of experimental and predicted results. *Int J Mach Tool Design Res*,4:347-365. doi:
- [19] Neo DWK, Liu K, Kumar AS. (2020) High throughput deep-hole drilling of Inconel 718 using PCBN gun drill. *Journal of Manufacturing Processes*,57:302-311. doi: 10.1016/j.jmapro.2020.06.043
- [20] Agmell M, Ahadi A, Ståhl J. (2013) The Link Between Plasticity Parameters and Process Parameters in Orthogonal Cutting. *Procedia CIRP*,8:224-229. doi: 10.1016/j.procir.2013.06.093

Figures

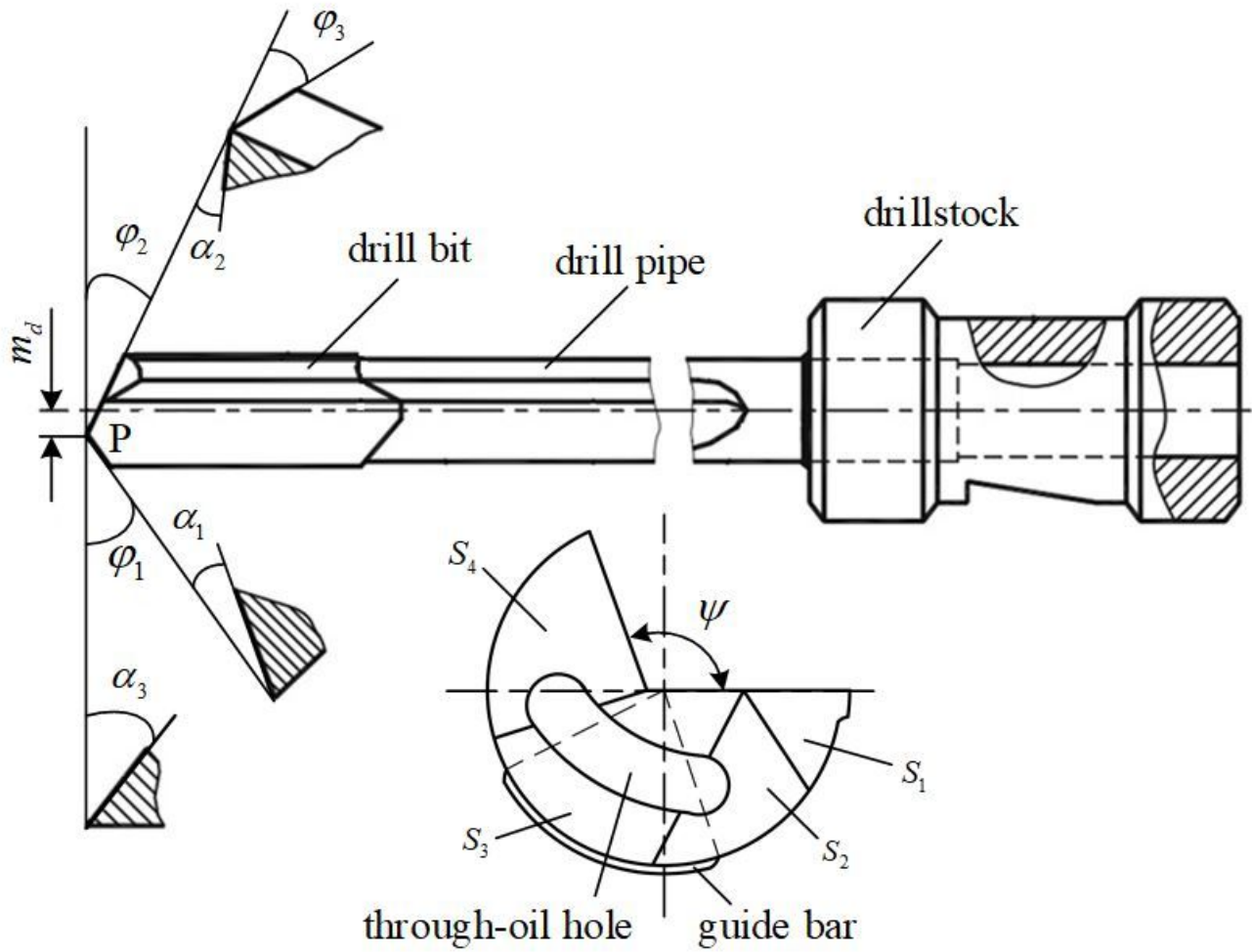


Figure 1

Schematic diagram of gun drill

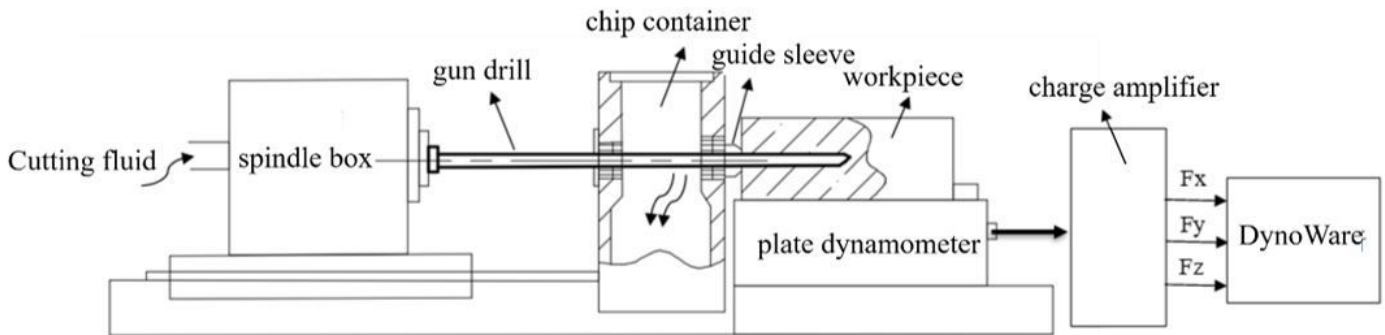


Figure 2

Schematic diagram of gun drill drilling force measurement test platform

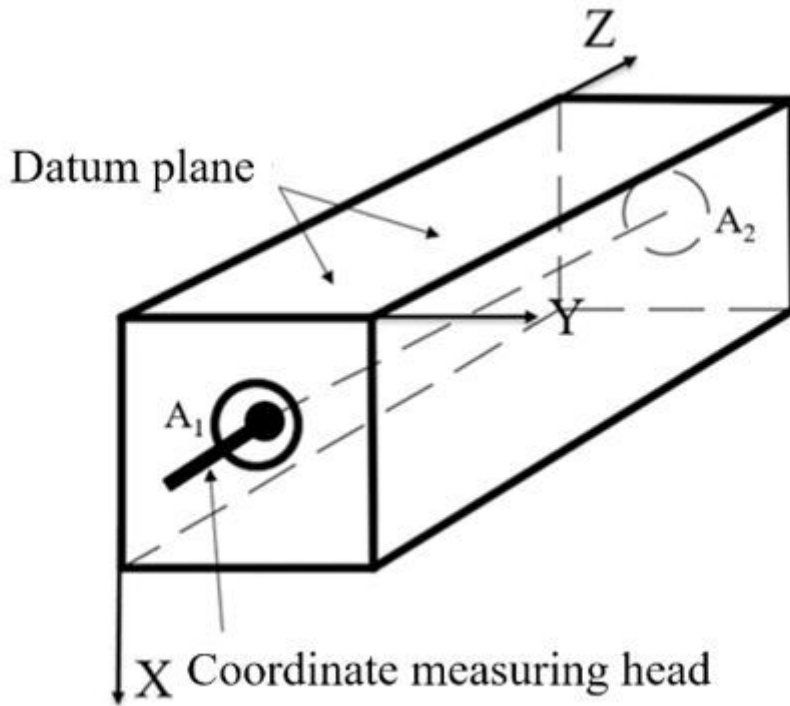


Figure 3

Sketch of workpiece coordinate system



Figure 4

Sketch map of surface roughness measurement position

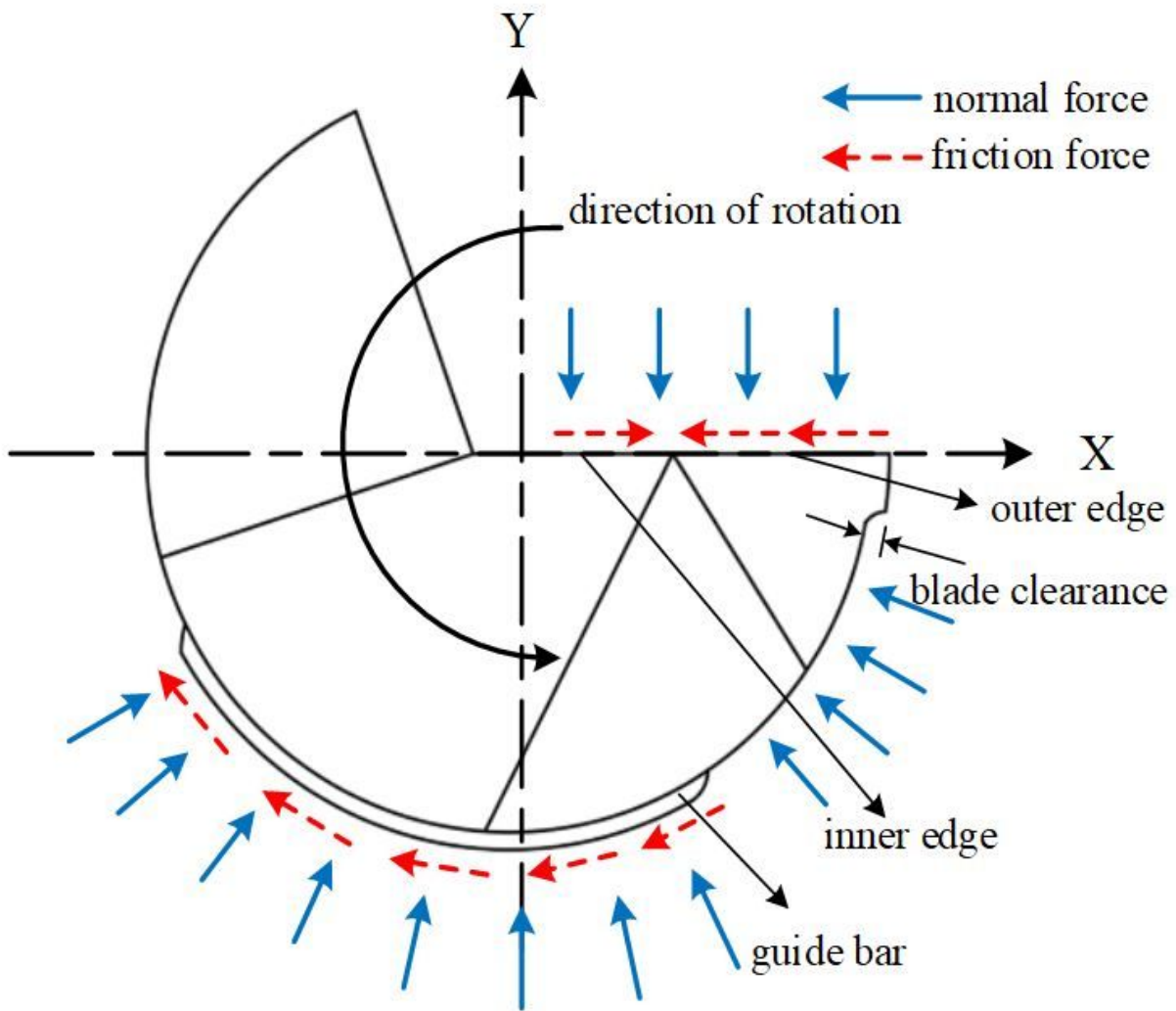


Figure 5

Analysis of the overall stress of the drill bit

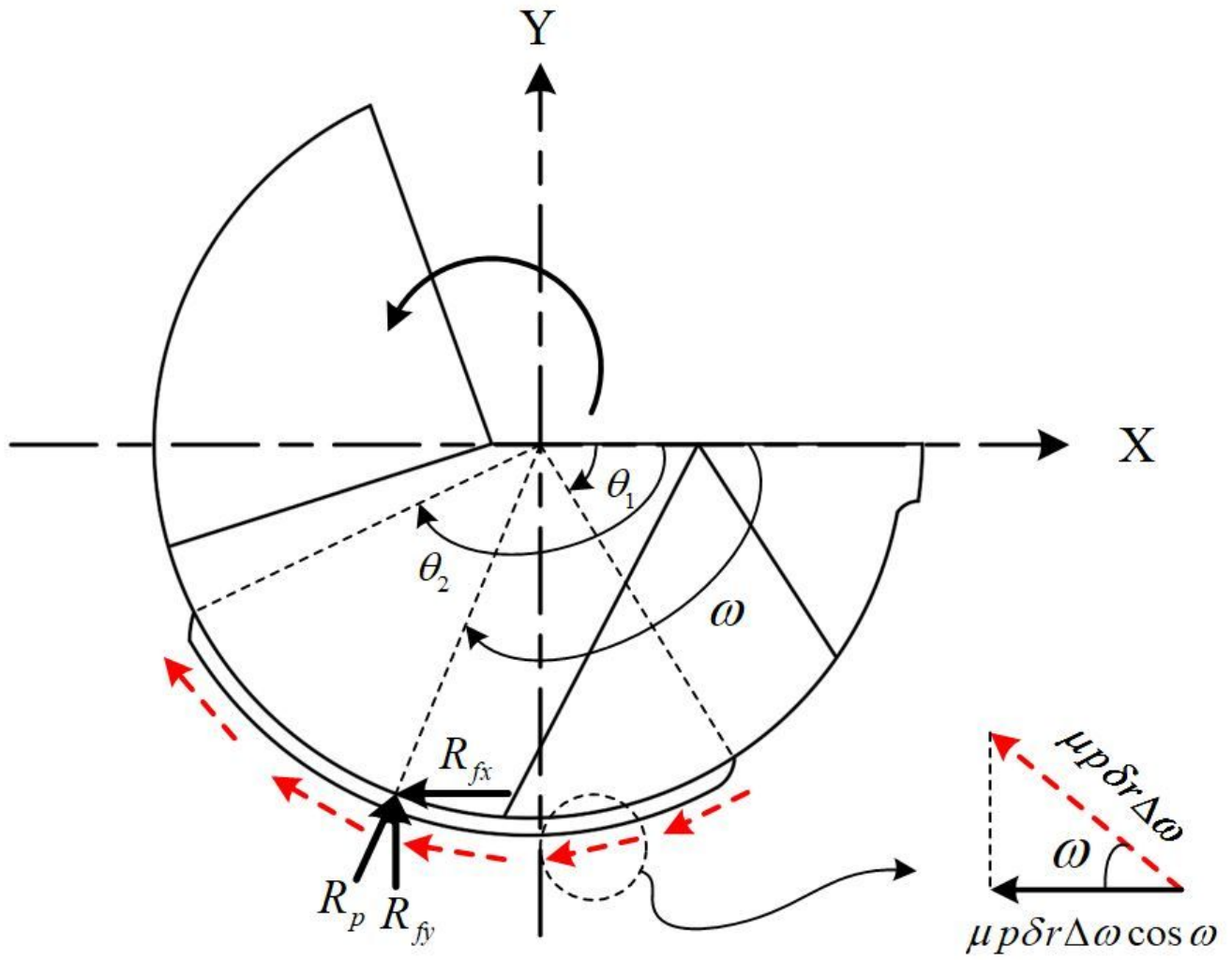


Figure 6

Simplified force decomposition on guide bar

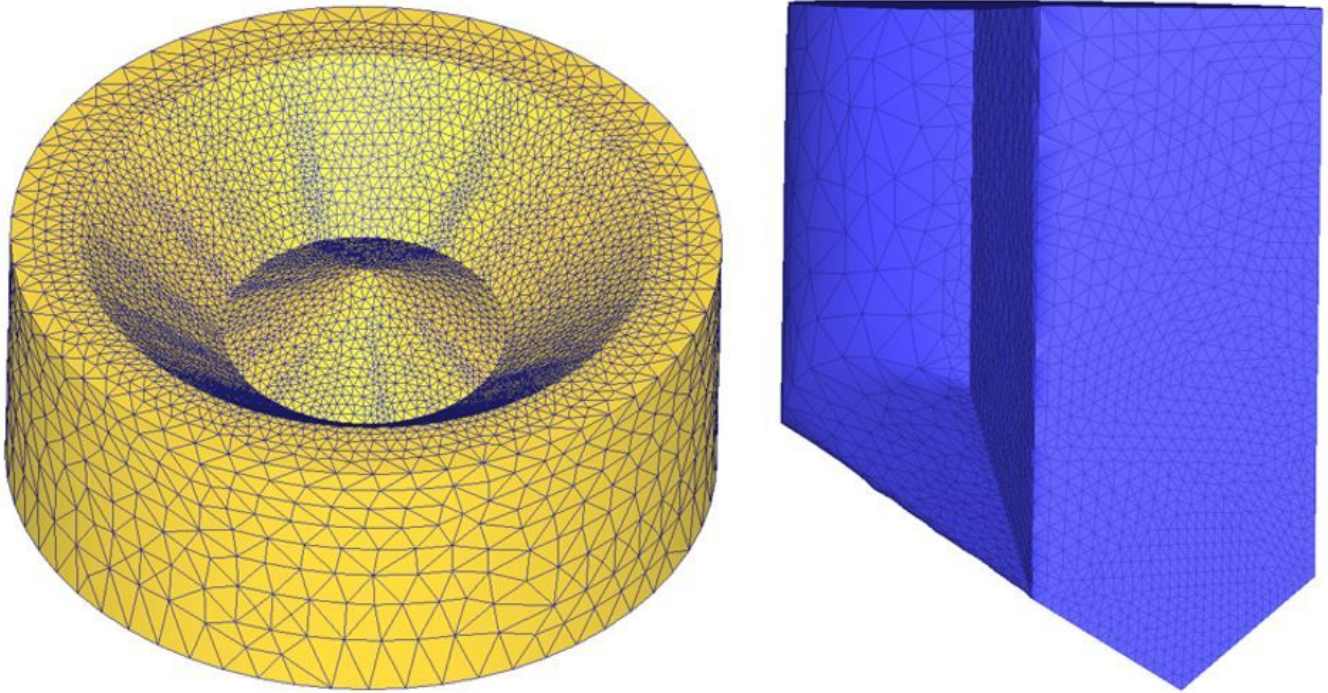


Figure 7

Effect drawing of mesh division of workpiece and tool

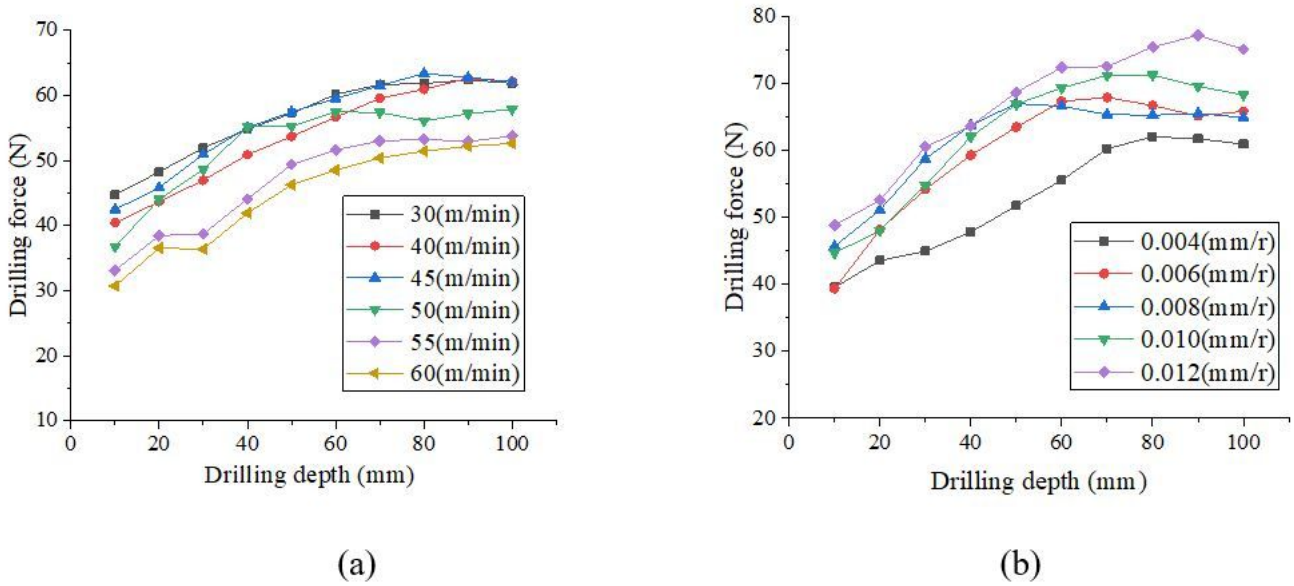
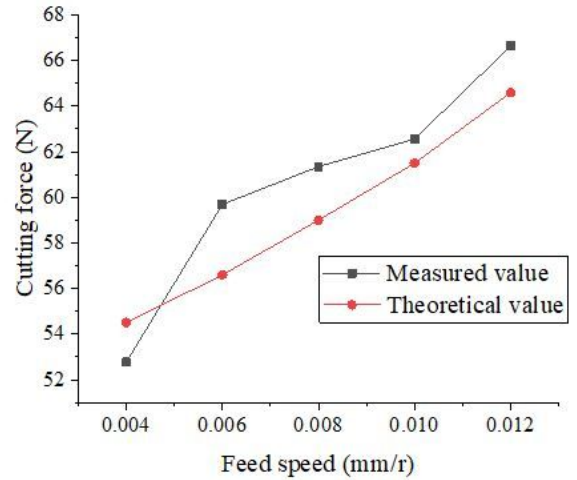
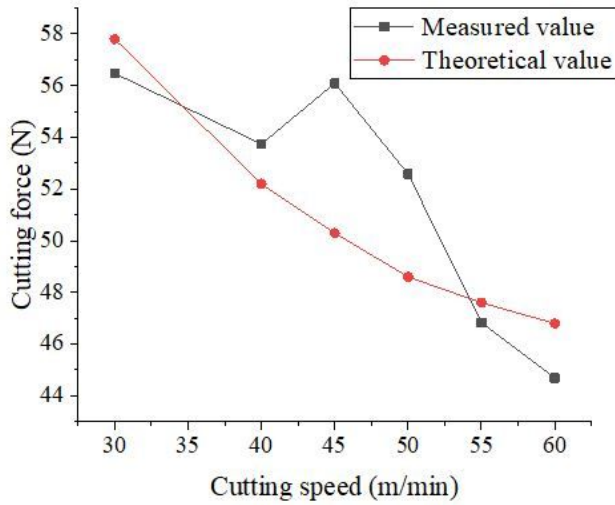


Figure 8

Comparison of drilling force with hole depth under different cutting speed (a) and feed speed (b)



(a)

(b)

Figure 9

Comparison of drilling force and cutting speed (a) and feed speed (b)

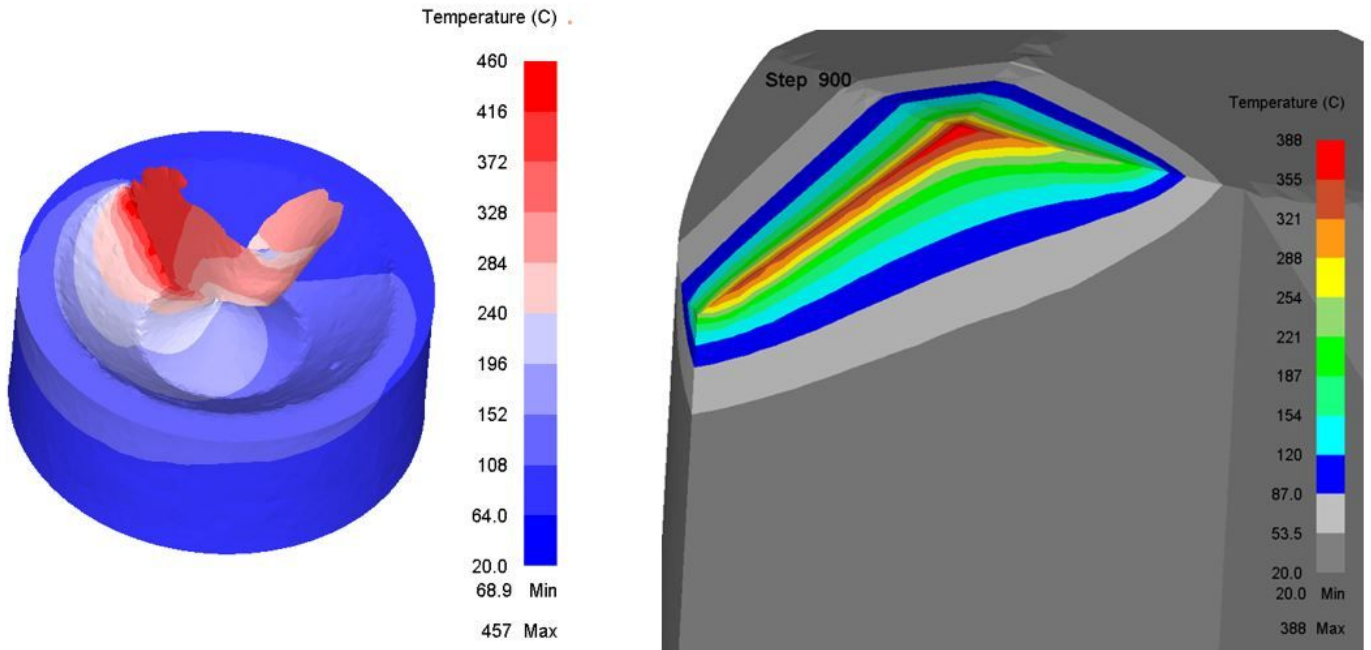


Figure 10

Temperature distribution nephogram of workpiece and tool at step = 900

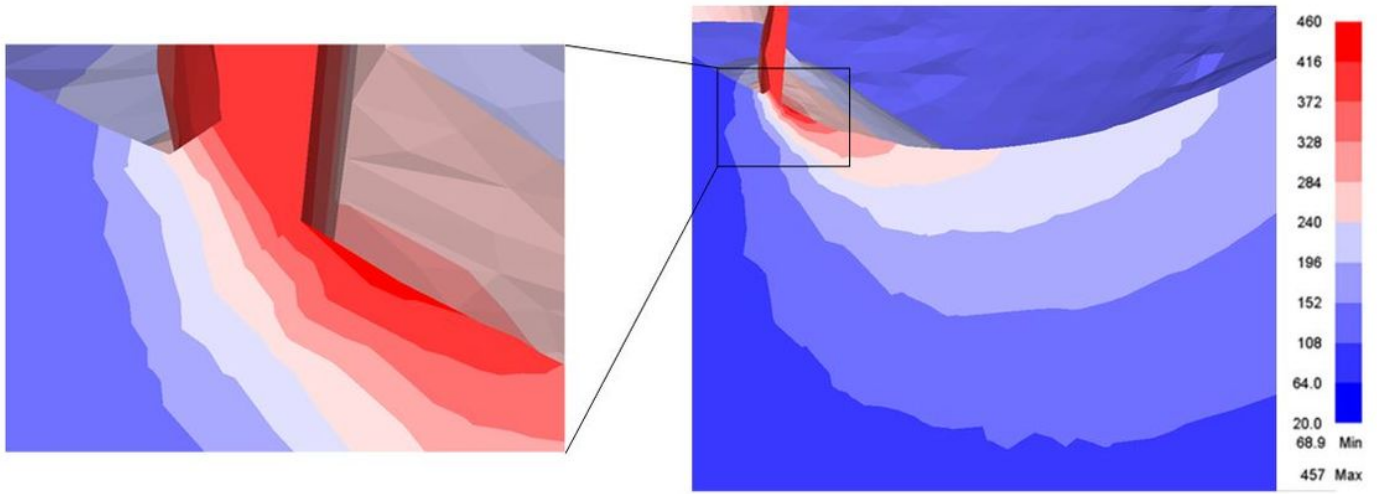


Figure 11

Distribution of workpiece temperature field along depth

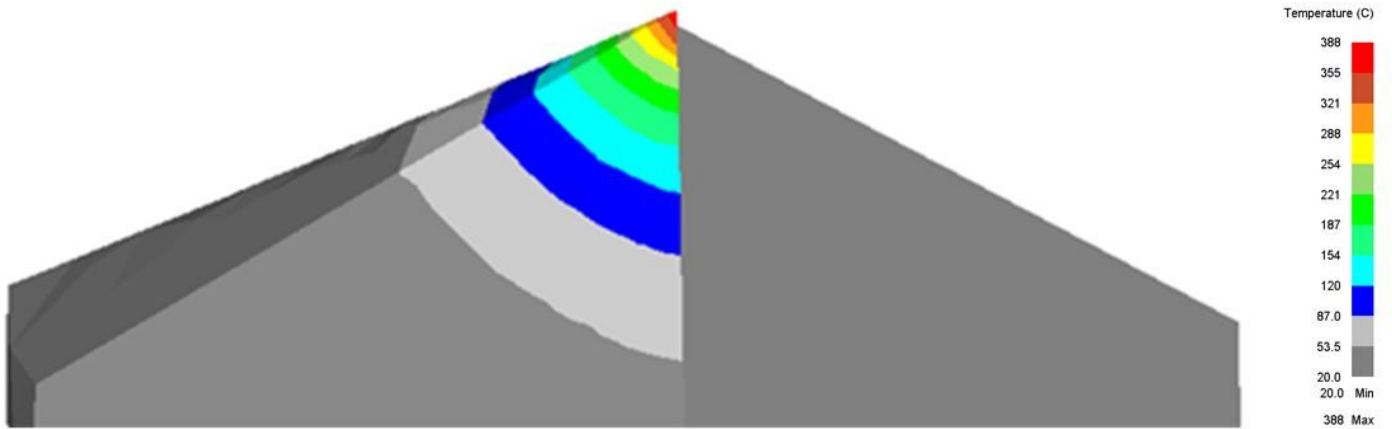


Figure 12

Cloud chart of temperature field along axial depth on bit

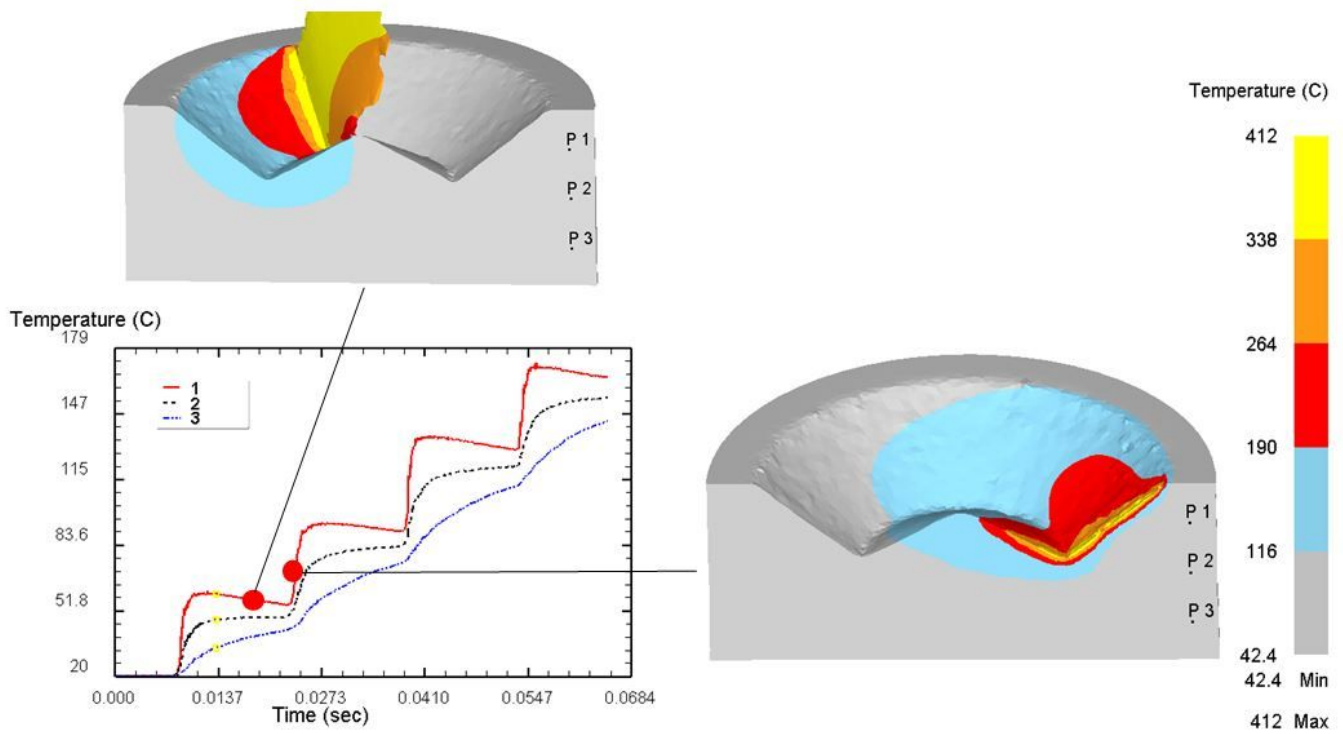


Figure 13

Temperature variation curve of internal reference point of workpiece

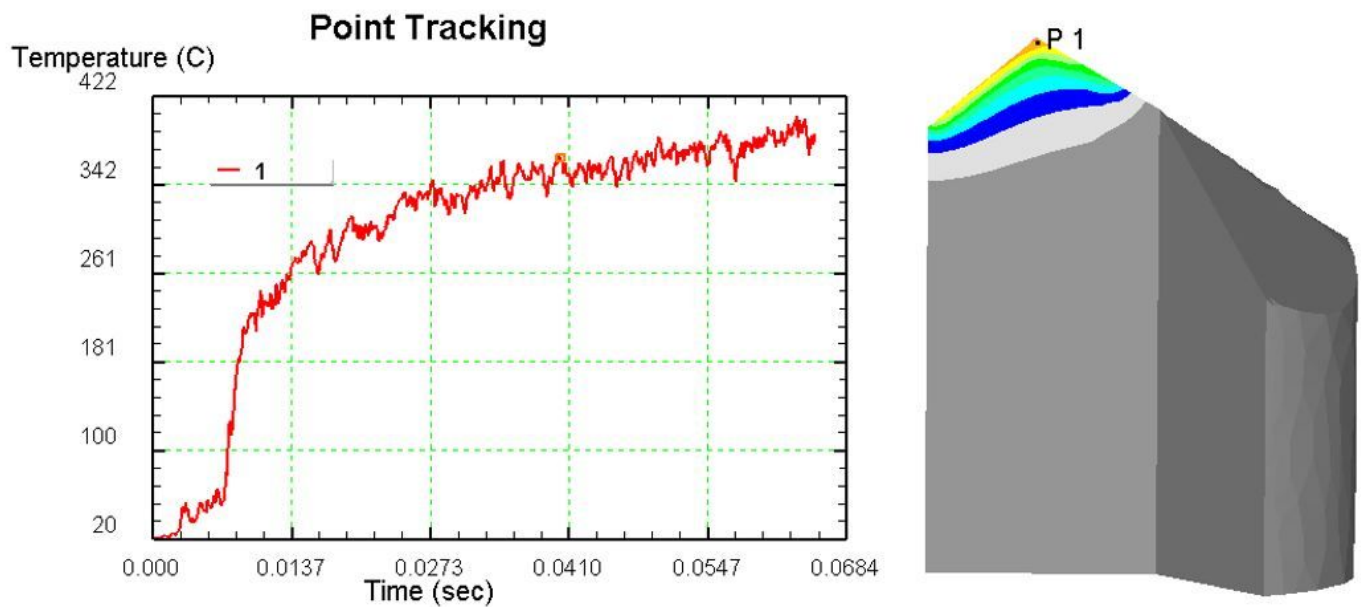


Figure 14

Cutting temperature curve with time at drill point

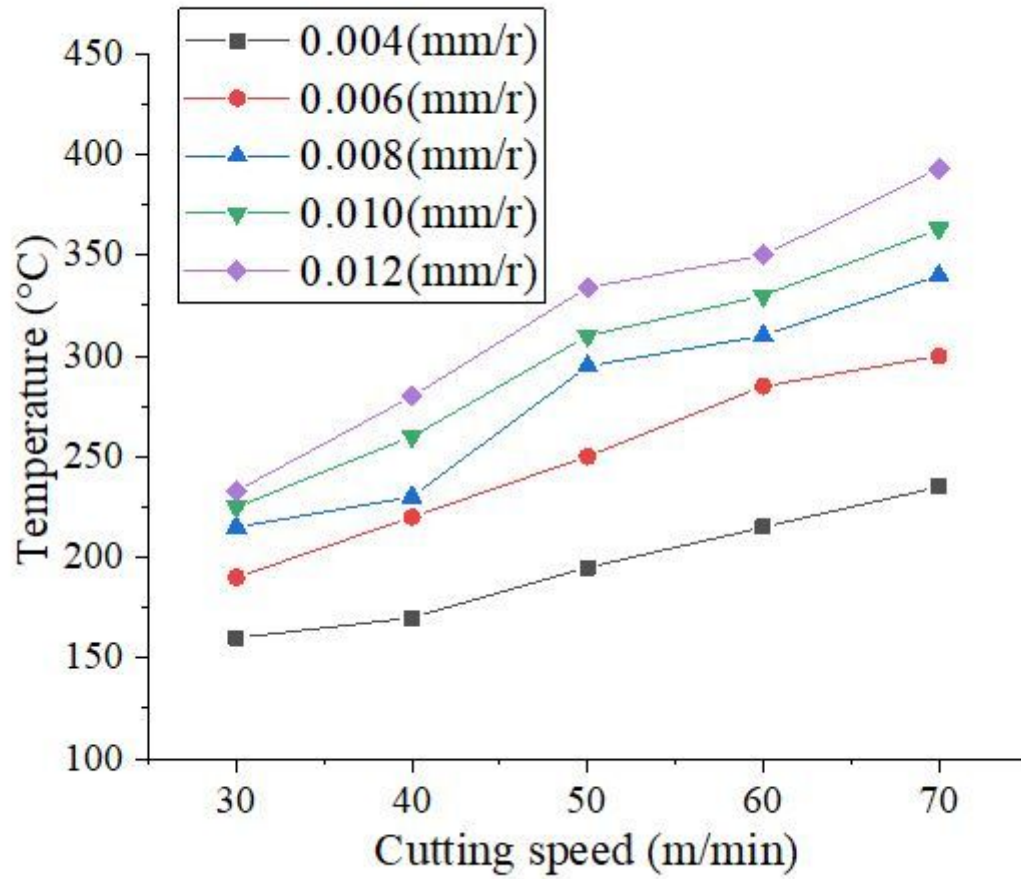


Figure 15

Comparison of cutting temperature and cutting speed under different feed speed

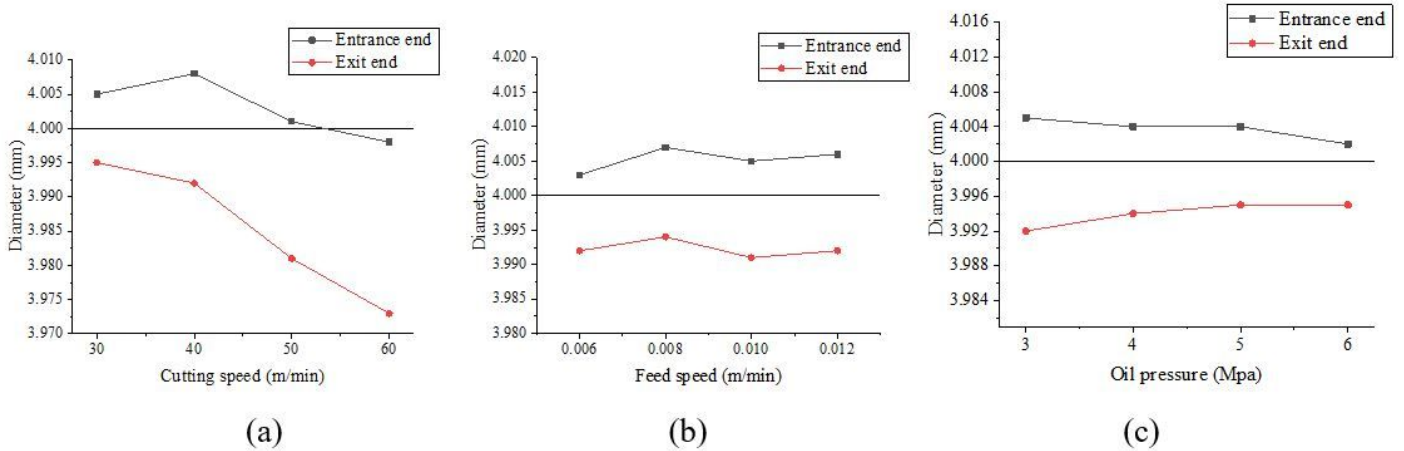


Figure 16

Comparison of diameter of hole inlet and outlet and cutting speed (a), feed speed (b) and oil pressure (c)

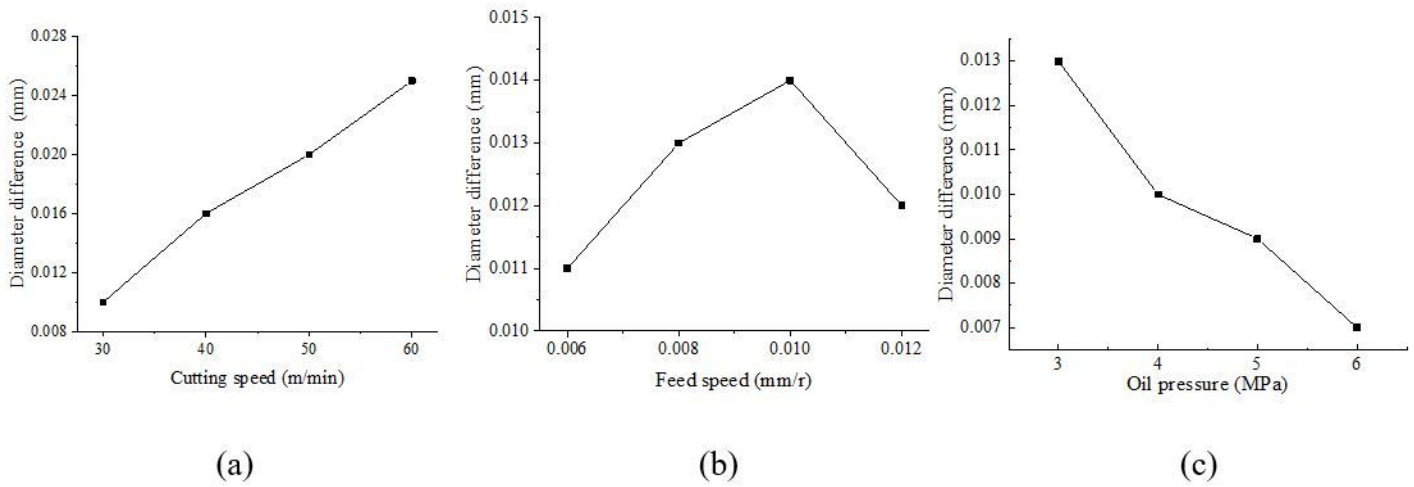


Figure 17

Comparison of diameter difference between inlet and outlet and cutting speed (a), feed speed (b) and oil pressure (c)

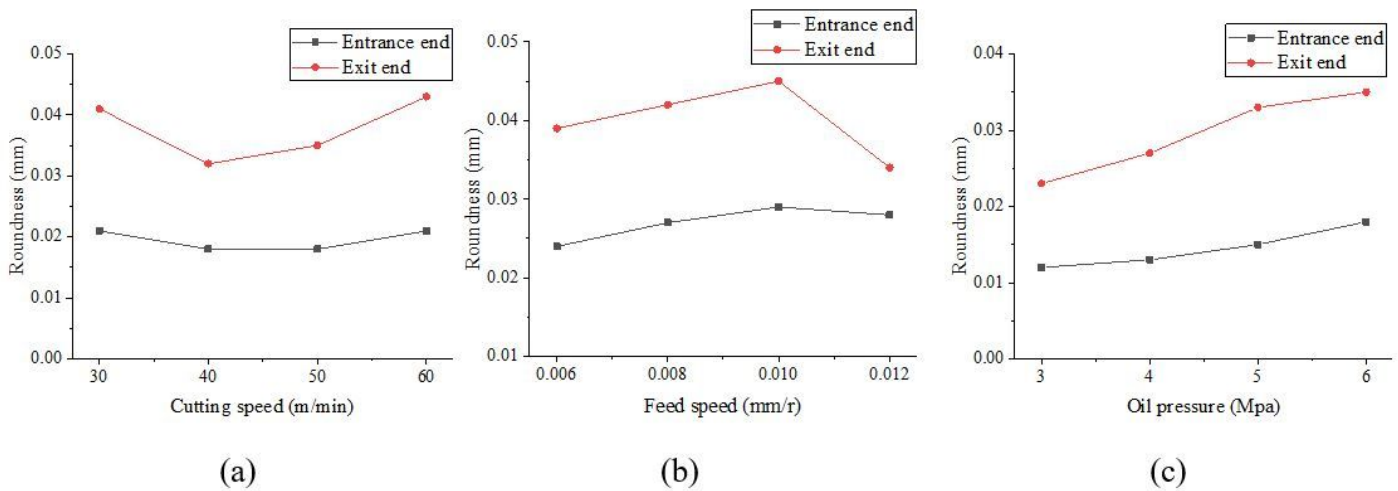


Figure 18

Comparison of roundness of hole inlet and outlet and cutting speed (a), feed speed (b) and oil pressure (c)

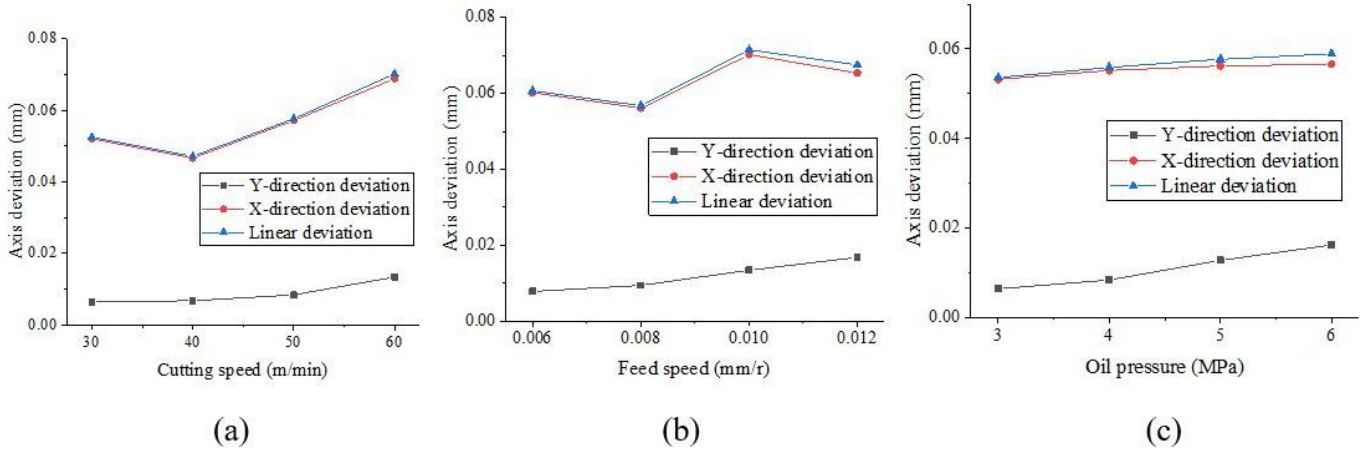


Figure 19

Comparison of axis deviation and cutting speed (a), feed speed (b) and oil pressure (c)

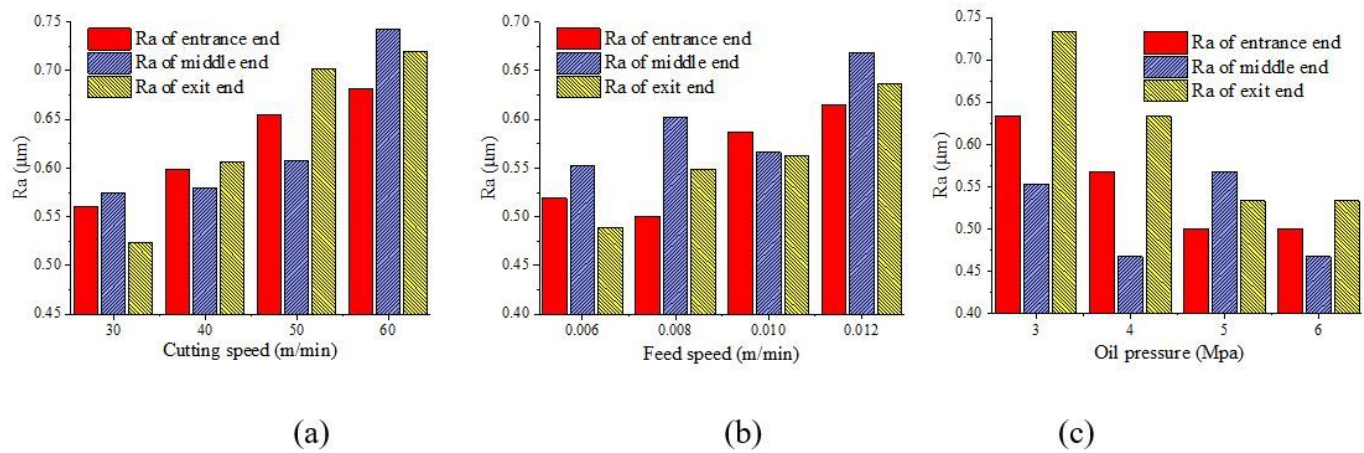


Figure 20

Comparison of surface roughness and cutting speed (a), feed speed (b) and oil pressure (c)